

Dust radiative forcing in snow of the Upper Colorado River Basin:

1. A 6 year record of energy balance, radiation, and dust concentrations

Thomas H. Painter,^{1,2,3} S. McKenzie Skiles,^{2,3} Jeffrey S. Deems,^{4,5} Ann C. Bryant,⁶ and Christopher C. Landry⁷

Received 27 February 2012; revised 25 May 2012; accepted 7 June 2012; published 26 July 2012.

[1] Dust in snow accelerates snowmelt through its direct reduction of snow albedo and its further indirect reduction of albedo by accelerating the growth of snow grains. Since the westward expansion of the United States that began in the mid-19th century, the mountain snow cover of the Colorado River Basin has been subject to five-fold greater dust loading, largely from the Colorado Plateau and Great Basin. Radiative forcing of snowmelt by dust is not captured by conventional micrometeorological measurements, and must be monitored by a more comprehensive suite of radiation instruments. Here we present a 6 year record of energy balance and detailed radiation measurements in the Senator Beck Basin Study Area, San Juan Mountains, Colorado, USA. Data include broadband irradiance, filtered irradiance, broadband reflected flux, filtered reflected flux, broadband and visible albedo, longwave irradiance, wind speed, relative humidity, and air temperatures. The gradient of the snow surface is monitored weekly and used to correct albedo measurements for geometric effects. The snow is sampled weekly for dust concentrations in plots immediately adjacent to each tower over the melt season. Broadband albedo in the last weeks of snow cover ranged from 0.33 to 0.55 across the 6 years and two sites. Total end of year dust concentration in the top 3 cm of the snow column ranged from 0.23 mg g⁻¹ to 4.16 mg g⁻¹. These measurements enable monitoring and modeling of dust and climate-driven snowmelt forcings in the Upper Colorado River Basin.

Citation: Painter, T. H., S. M. Skiles, J. S. Deems, A. C. Bryant, and C. C. Landry (2012), Dust radiative forcing in snow of the Upper Colorado River Basin: 1. A 6 year record of energy balance, radiation, and dust concentrations, *Water Resour. Res.*, 48, W07521, doi:10.1029/2012WR011985.

1. Introduction

[2] The runoff from the Colorado River supplies water to over 30 million people in seven United States and Mexico. Climate change projections suggest that this runoff will decrease in the next 50 years by 7–20% due to increases in evapotranspiration and decreases in the ratio of snowfall to rain [Christensen and Lettenmaier, 2007; Barnett and Pierce, 2009]. Such scenarios challenge the

sustainability of the freshwater supply to the southwest United States [MacDonald, 2010].

[3] Recent research however has shown that radiative forcing by dust in snow has been shortening snow cover duration by several weeks due to a 5–7-fold increase in dust loading since the period prior to the European-settlement of the western United States in the mid-1800s [Painter *et al.*, 2007; Neff *et al.*, 2008]. Extended to the scale of the Upper Colorado River Basin, this impact has brought peak normalized runoff at Lee's Ferry, Arizona (Lake Powell) more than three weeks earlier and reduced the total annual runoff by an average of ~5% [Painter *et al.*, 2010].

[4] Based on this new understanding of dust's influence on snow cover, water managers in the Upper Colorado basin now seek detailed real-time knowledge of dust presence, radiative forcing, and its potential to accelerate snowmelt, as well as understanding its implications for water supply under current conditions and in a changed climate. Likewise, water stakeholder groups, water conservation districts, and state and federal agencies are discussing efforts to restabilize soil surfaces in the dust-emitting regions to mitigate impacts of dust on snowmelt and runoff.

[5] Growing field observations and modeling simulations also suggest that increases in dust and black carbon deposition to snow in the Hindu Kush-Himalaya lead to retreat

¹Jet Propulsion Laboratory, California Institute of Technology, Pasadena, California, USA.

²Department of Geography, University of California, Los Angeles, California, USA.

³Joint Institute for Regional Earth System Science and Engineering, University of California, Los Angeles, California, USA.

⁴National Snow and Ice Data Center, Boulder, Colorado, USA.

⁵NOAA Western Water Assessment, Boulder, Colorado, USA.

⁶Department of Geography, University of Utah, Salt Lake City, Utah, USA.

⁷Center for Snow and Avalanche Studies, Silverton, Colorado, USA.

Corresponding author: T. H. Painter, Jet Propulsion Laboratory, California Institute of Technology, 4800 Oak Grove Dr., Pasadena, CA 91109, USA. (thomas.painter@jpl.nasa.gov)

and downwasting of glaciers [Ramanathan *et al.*, 2007; Kaspari *et al.*, 2009]. These results along with studies of the damaging health impacts of black carbon and other industrial pollutants have led to recent statements from the United Nations Environment Programme [United Nations Environmental Programme/World Meteorological Organization, 2011], the Vatican Pontifical Academy of Sciences [Ajai *et al.*, 2011], and the U.S. Department of State's initiation of the Climate and Clean Air Coalition to Reduce Short-Lived Climate Pollutants about the need to reduce atmospheric and cryosphere loading of carbonaceous particles. The studies that support these statements however have been performed without sustained in situ or remotely sensed observations of the variation of radiative forcing in snow, except for the present measurements.

[6] As these policy-related activities grow, it is imperative that we improve our understanding of the interannual variability of dust loading, the radiative forcing by dust, and the impacts on snowmelt. In 2003/2004, a collaboration between the lead author and coauthor Landry, Executive Director of the Center for Snow and Avalanche Studies (Silverton, Colorado), established two energy balance and detailed radiation towers in the Senator Beck Basin Study Area (SBBSA). The SBBSA is a research catchment in the headwaters of the Uncompahgre River of the Upper Colorado River Basin and is maintained and sampled by the Center for Snow and Avalanche Studies.

[7] The instrumentation on the towers was specifically designed and configured to facilitate energy balance modeling of the snowpack and assess the relative impacts of radiative forcing by dust, climate change, and climate variability. Along with energy balance data from a sibling tower on the Grand Mesa, Colorado (installed in the Fall of 2009), these are the only comprehensive energy balance and detailed radiation data for snow in the Upper Colorado River Basin. As such, they uniquely allow us to answer the question of how much does radiative forcing by dust deposition impact the energy balance and snowmelt of the mountain snowpack. In this paper, we present 6 years of dust loading data, meteorology, and detailed radiation data from the SBBSA. In the partner paper [Skiles *et al.*, 2012], we present the retrievals of dust radiative forcing in snow and investigate the impacts of that forcing and atmospheric warming on the acceleration of snowmelt.

2. Background

[8] Melting energy for mountain snow (in all but closed-canopy forest environments) comes primarily from net solar radiation, itself controlled by changes in irradiance and snow albedo [Oerlemans, 2000; Bales *et al.*, 2006; Painter *et al.*, 2007]. Snow albedo is controlled by changes in snow grain size (described by either optical grain size or specific surface area) and by light absorbing impurities such as dust, black carbon, and tree litter. Snow grain growth decreases snow albedo in the near-infrared (0.7 to 1.5 μm) and shortwave-infrared wavelengths (1.5 to 3.0 μm) whereas the light-absorbing impurities generally decrease the spectral albedo in the visible wavelengths (0.4 to 0.7 μm) (Figure 1).

[9] The spectral albedo of clean snow has values greater than 0.95 in the visible wavelengths but can drop to near

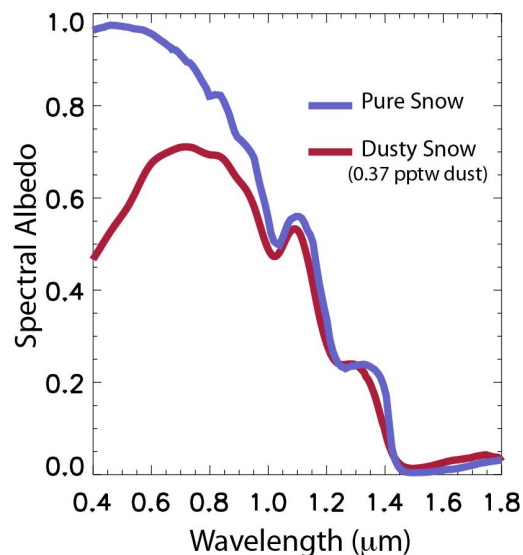


Figure 1. Spectral albedo of clean snow (modeled) and snow with dust concentration of 0.37 parts per thousand by weight of snow water or mg g^{-1} (measured).

0.0 in the shortwave infrared wavelengths. Increases in grain size decrease the spectral albedo primarily in the range from 0.7 to 1.5 μm . These changes drive the decrease in broadband albedo for clean snow. However, absorbing impurities such as dust and carbonaceous particles decrease the spectral albedo in the visible wavelengths, from 0.95–0.98 down to as low as 0.30. Together, grain growth and absorbing impurities arguably give snow the greatest range of albedo of any surface on Earth.

[10] The dust and carbonaceous particles are heated by absorption of solar radiation and, in turn, they heat the surrounding snow primarily through conduction to the contiguous snow grains. Once the surrounding snow is at 0°C , the additional radiative forcing contributes to melting of those grains. Timing of deposition of impurities and persistence at or near the snow surface determines their influence on snowmelt. Dust that is deposited during midwinter events is usually buried by subsequent snow accumulation, limiting the amount of time it spends at or near the snow surface absorbing solar radiation. Importantly, the particle size of dust is generally large enough that it is not entrained in snowmelt and washed to deeper layers away from its radiative forcing capacity [Higuchi and Nagoshi, 1977; Conway *et al.*, 1996]. Instead, the dust remains in its layer while overlying snow melts and percolates to below the dust. As overlying dust layers merge with those previously buried, the visible spectral albedo decreases further, increasing radiative forcing and snowmelt. Spring often brings further dust events, which accelerate snowmelt through their direct reduction of albedo, and further reduce snow albedo by accelerating the growth of snow grains.

3. Study Area, Instrumentation, and Observations

[11] We present data from two micrometeorological stations measuring energy balance and radiation fluxes in the

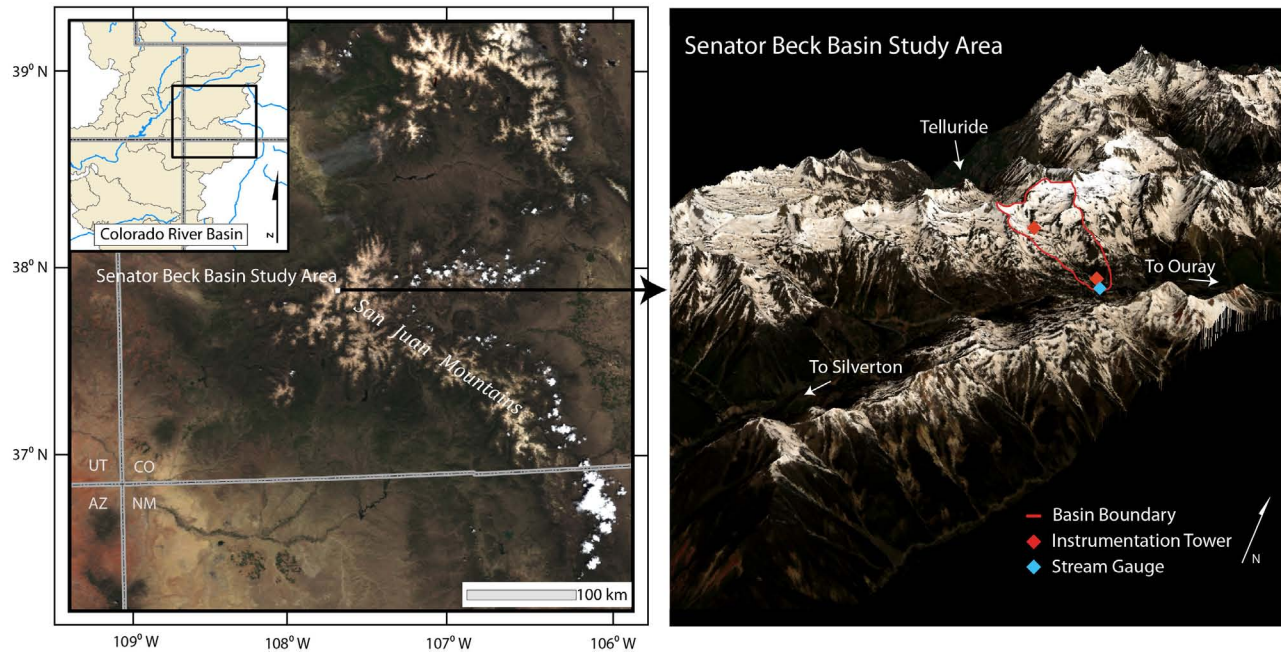


Figure 2. Overview of the Senator Beck Basin Study Area. The Swamp Angel Study Plot and Senator Beck Study Plot are indicated.

Senator Beck Basin Study Area (SBBSA), western San Juan Mountains in the Upper Colorado River Basin ($37^{\circ} 54' 30''$ N, $107^{\circ} 43' 30''$ W) (Figure 2). The SBBSA lies in a generally east-facing basin with the stations in the alpine and the subalpine. As the first two complete energy balance and detailed radiation stations in the Upper Colorado River Basin, they uniquely generate knowledge of snowmelt dynamics in that region. In 2009, we added a similarly instrumented tower on the Grand Mesa of Colorado, ~ 150 km to the north.

[12] The alpine site, Senator Beck Study Plot (SBSP), sits on level tundra at 3719 m with a 10 m instrument tower and a 12 m by 36 m snow profile plot in which snow properties and dust concentrations are observed regularly (Figure 3a). The site is exposed to strong winds and its measurements are considered representative of a wind-affected snow cover setting.

[13] The subalpine Swamp Angel Study Plot (SASP) is located in a wind-protected forest clearing at 3368 m (Figure 3b). Wind speeds are much lower than at the alpine site and wind redistribution of snow cover is negligible. The study site contains a $30 \text{ m} \times 30 \text{ m}$ snow profile plot, a storage precipitation gauge, and a 6 m tower holding the same instrumentation array as on the SBSP tower. The Senator Beck Stream Gauge (SBSG) is located about 100 m downstream of the subalpine tower at the basin outlet.

[14] The towers are instrumented with up- and down-looking broadband solar and filtered near-infrared/shortwave-infrared pyranometers (Kipp&Zonen CM21 and Kipp&Zonen CM21 with Schott RG695 glass filters), up-looking longwave pyrgeometers (Kipp&Zonen CG4), and down-looking surface temperature sensor for estimating snow-emitted longwave radiation (AlpuG GmbH SnowSurf). Wind speed, wind direction, air temperature, and relative humidity are measured every 5 s at two heights (RM YoungTM model 05,103-5 and Campbell ScientificTM CS500). Snowpack depth at both

towers is measured at the end of each hour by an ultrasonic distance sensor (Campbell ScientificTM SR50).

[15] Precipitation (mm) is measured at the subalpine site in an open topped collector; accumulated fluid is weighed every 5 s and reported hourly. Precipitation is not measured at the alpine site because of frequent high winds that would under sample snowfall. All subhour measurements are averaged hourly and daily. A hexagonal array of vertical 3 m snow depth measurement stakes are deployed around the tower at a radius of 7.5 m to calculate the snow surface gradient to allow correction of incident radiation measured by the level up-looking pyranometers and in turn the calculation of albedo (Table 1).

[16] Dust loading and dust concentrations are sampled within the alpine and subalpine snow study plots for each dust event. We sample dust layers, as soon after deposition as site access is possible and safe from avalanches. The dust loading is determined by collecting the dust layer and some clean snow above and below the layer in a column over a 0.5 m^2 area. These samples are melted, dried, and preserved, and single event dust mass flux is recorded (g m^{-2}). For each event, an additional bulk sample of dust mass (sample size dependent on volume of observer's backpack) is collected for texture and chemical analysis. The Earth Surface Processes Laboratory of the United States Geological Survey, Colorado, performs the texture and chemical analyses. The results from these analyses have been presented in the work of Lawrence *et al.* [2010]. These analyses reveal that dust deposited here is composed of primarily silt- and clay-sized particles, consistent with the observations that the dust sources are regional. The dust has composition of 8% organics and 92% mineral matter, with enrichments of heavy metals including As, Cu, Cd, Mo, Pb, and Zn.

[17] Regular sampling of snow pits within the study plot boundaries is used to monitor the thermal and metamorphic



Figure 3. Energy balance/radiation towers. (a) Senator Beck Study Plot (alpine site), 12 May 2009. (b) Swamp Angel Study Plot (subalpine site), 13 May 2009.

state of the snowpack and layering of dust concentration. Pits are sampled monthly during the winter and weekly during the ablation season, with specific timing of observations subject to avalanche conditions. Weekly sampling

generally starts in mid-March. In order to understand the relationship between snow albedo at the meteorological stations and dust concentration in the near surface layers of the snowpack, we collect the top 30 cm of the snowpack at

Table 1. Energy Balance and Radiation Measurements

Measurement/Instrument/Range	Subalpine	Alpine
Up/down broadband shortwave fluxes; Kipp&Zonen CM21 pyranometer; 0.285–2.800 μm	•	•
Up/down filtered shortwave fluxes; Kipp&Zonen CM21 pyranometer w/RG695 glass; 0.695–2.800 μm	•	•
Longwave irradiance; Kipp&Zonen CG4 pyrgeometer; 4.500–42.000 μm	•	•
Snow surface temperature; AlpuG GmbH SnowSurf	•	•
Air temperature and relative humidity; Campbell/Vaisala CS500-U (2 heights)	•	•
Wind speed and direction; RM Young 05,103-5 (2 heights)	•	•
Barometric Pressure; Campbell/Vaisala PTB101B (CS105)	•	•
Precipitation; ETI Instrument Systems Noah II	•	

3 cm intervals with horizontal area of 500 cm² (Figure 4), 30 cm being the nominal limit of shortwave radiation penetration into the snowpack. These 3 cm × 500 cm² snow samples are melted and filtered with individually pre-weighed 0.495 μm Nuclepore pore diameter filters. With the differential dust mass and the total snow sample mass, we report the dust concentration in milligram of dust per gram of snow sample (mg g⁻¹). The last sampling of the season occurs just prior to snowpack depletion when dust from all events has generally converged at the surface (except perhaps those that may have occurred just at the beginning of snowfall). Because dust is generally not entrained in melt, we use these samples to report end of year dust concentration. To determine the total dust load for the snow cover period, we sum the dust masses across all layers of the last snow pit before complete melt and multiply the 0.05 m² area by 20 to report the column dust load in grams per meter squared (g m⁻²). This method is of course sensitive to spatial variability and this sensitivity motivates emerging remote sensing technology that will allow us to determine the spatial variation in dust radiative forcing and refined estimates of total loading.

[18] Given that the gradient of the snow surface beneath the down-looking pyranometers changes by snow accumulation, wind redistribution and heterogeneous snowmelt, calculations of snow albedo with the uncorrected radiation flux measurements (i.e., assuming a level snow surface) can be erroneous. The up- and down-looking pyranometers

are both estimated to be level to within 1°, given design and installation. Therefore, the up-looking pyranometer measures the hemispherical irradiance onto a level surface. The direct ratio of the reflected flux with the irradiance measurement for albedo assumes that the down-looking pyranometer measures flux from a level surface. However, the snow surfaces at the subalpine and alpine towers are never level while snow covered (Figure 5) and therefore, the uncorrected ratio for albedo introduces a severe asymmetric artifact to the diurnal cycle of albedo (Figure 6). *Jonsell et al.* [2003] give an excellent description of this effect and the asymmetries of albedo calculations.

[19] We determine the slope and aspect of the snow surface with an array of graduated snow stakes that are referenced to an origin at the ground surface immediately beneath the down-looking broadband pyranometer and the sonic snow depth sensor. At the subalpine tower we have 4 stakes and the sonic depth sensor for a total of 5 measurements. Because of the stronger wind redistribution and variability of snow surface slope and aspect at the alpine tower (Figure 5), we have 6 stakes and the sonic depth sensor for a total of 7 measurements. On a weekly basis, a Center for Snow and Avalanche Studies observer visits each site and notes the snow depth at each stake, and snow depth is recorded on an hourly basis with the sonic depth sensor. The time series of snow depths at each stake and each sonic depth sensor is interpolated linearly between each measurement to a daily time step. For each day, we then determine



Figure 4. Snowpit sampling for stratigraphy of dust concentration, 7 May 2009.

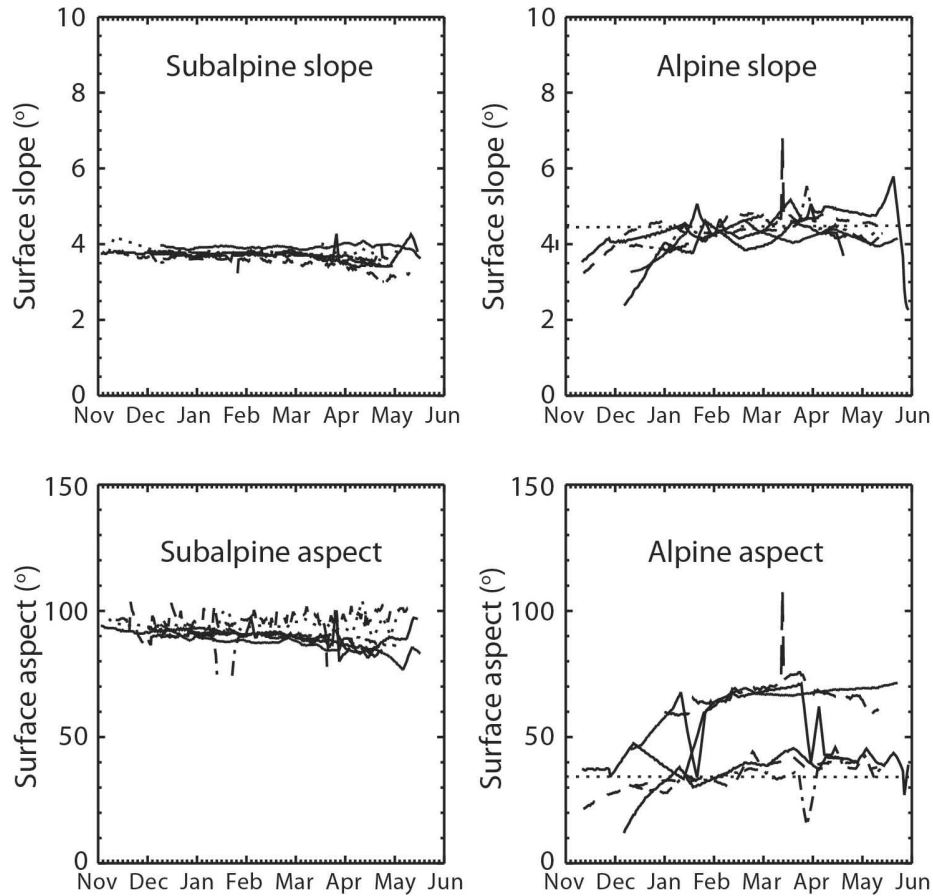


Figure 5. Time series of snow surface geometry for all years in 2005–2010. (a) Subalpine slope. (b) Alpine slope. (c) Subalpine aspect. (d) Alpine aspect. Aspect referenced clockwise from north, such that east is 90° and west is 270°.

the best fit of a plane to the snow depth arrays. The gradient of this plane gives the surface to which we correct the broadband and NIR/SWIR irradiances. We then correct albedo according to the following relationships (Figure 6):

$$\cos \beta = \cos \theta_s \cos \theta_n + \sin \theta_s \sin \theta_n \cos \{\phi_s - \phi_n\}, \quad (1)$$

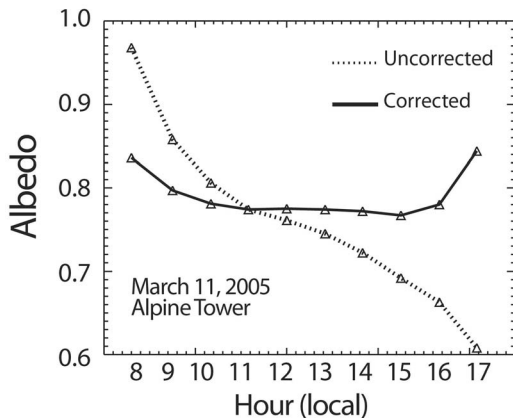


Figure 6. Correction of diurnal variation in snow albedo at the alpine site, using the slope and aspect data in Figure 5.

where β is the local solar zenith angle, θ_s is the solar zenith angle for a horizontal surface, ϕ_s is the solar azimuth angle, θ_n is the surface slope, and ϕ_n is the surface aspect. The scalar by which we correct the measured downward irradiances to at-surface irradiances is given by

$$M_\beta = \frac{\cos(\beta)}{\cos(\theta_s)}. \quad (2)$$

The direct proportion of the surface irradiance, the proportion of the total irradiance as determined from modeling of the potential irradiance with the Santa Barbara DISORT Atmospheric Radiative Transfer (SBDART), is scaled by M_β and added back to the diffuse irradiance. We assume that the diffuse irradiance is relatively unchanged with slope and aspect. This assumption is being tested in other work but the correction of albedos suggests that it is valid.

[20] Wind speeds are markedly lower at the subalpine site. When snow accumulates on the up-looking pyranometers, it occludes the irradiance from the pyranometer. The sensor then reports irradiances that are often lower than the reflected fluxes. When this is the case, we correct these irradiances by assuming that the albedo at the subalpine site ($\alpha_{subalpine}$) is the same as at the alpine site (α_{alpine}). The basis for this assumption is that snow occlusion of the

up-looking pyranometers occurs when fresh snowfall has occurred. Our observations indicate that the albedos of new snow at the subalpine and alpine lie within 2% of each other without bias. Therefore, we back-calculate the subalpine broadband irradiance, $S_{subalpine}$, as follows:

$$S_{subalpine} = \frac{K_{subalpine,reflected}}{\alpha_{alpine}}, \quad (3)$$

where $K_{subalpine,reflected}$ is the measured reflected flux.

[21] We also measure aerosol optical depth and other atmospheric column properties at the subalpine site with a CIMEL sunphotometer. This sunphotometer has operated in the NASA Aerosol Robotic Network (AERONET) since the autumn of 2005 with modest interruptions. The site name is Red_Mountain_Pass and can be found on the AERONET website at http://aeronet.gsfc.nasa.gov/new_web/photo_db/Red_Mountain_Pass.html. The measurements from the Red_Mountain_Pass AERONET site will be described in a subsequent paper due to the complexity of these data.

4. Results

[22] We present the timing of dust deposition events, time series of concentrations, and the meteorological and energy balance results. Part 2 of this paper [Skiles *et al.*, 2012] presents the radiative forcing and snowmelt modeling results.

4.1. Timing of Dust Deposition to Snow

[23] Figure 7a shows the timing of dust deposition events to snow cover in the SBBSA for years 2005 through 2010 during the winter through spring. A dust deposition event is defined as that which can be observed by the eye in the mountain snowpack. Annual distributions are generally centered in April but with some distinct clustering. Deposition events in 2006 and 2007 spanned four months from winter into spring until the end of snow cover whereas events in 2008 through 2010 only spanned two months. Moreover, 2009 and 2010 saw by far the greatest dust loading in these more compressed periods but with shifted spans of 27 February to 25 April and 30 March to 22 May.

[24] Figure 7b gives the summary distribution by month across all dust to snow deposition events. While a few events occur in the late autumn, most events occur after the desert regions have dried from winter snowfall and rain but synoptic scale storms continue to bring precipitation to the region. It is clear that, across this period of record, the vast majority of events occur during March–April–May (MAM), dominated by events in April. The majority of snowfall in the mountains of the Upper Colorado occurs before the MAM period. Therefore, the timing of the majority of dust events is such that they remain closer to or at the snow-atmosphere interface where their radiative forcing and efficacy in accelerating snowmelt is maximized. Snow cover exists in the SBBSA generally from October through mid June.

4.2. Dust Concentrations

[25] Dust loading is partly driven by the number of dust events in a snow season, but the magnitude of dust loading is highly variable annually (Figure 8). It is near-snow surface dust concentration that governs the albedo reduction

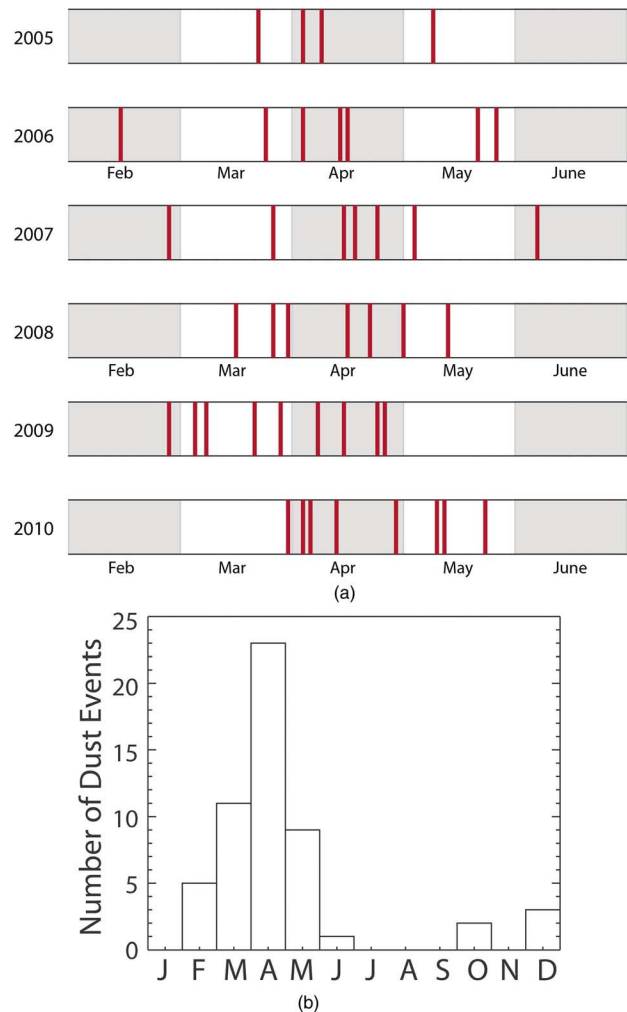


Figure 7. (a) Annual distributions of dust deposition events to snow cover in SBBSA across 2005 through 2010. (b) Histogram of dust deposition events in SBBSA across 2005 through 2010.

and radiative forcing, and as such the number of dust events is not necessarily a good predictor of end-of-year snow albedo or of dust radiative forcing (Figure 8). While we know the various controls of dust emission, transport, and deposition in isolation, we are still in the infancy of understanding their relative contributions. We differentiate those events that occur after 1 March to highlight those events that can have the greater radiative and snowmelt impact (Figure 8a) due to the longer period over which these dust layers exist on the snow surface. The number of dust deposition events increased quasi-monotonically over the period of our study (since 2005) (Figure 8b), whereas dust loading has not. For example, 2008 and 2009 had the same number of dust events after 1 March, respectively, but the end of snow cover dust concentration in 2009 (4.16 mg g^{-1}) was about 6 times greater than in 2008 (0.71 mg g^{-1}). The greatest end of snow cover dust concentrations occurred in 2009 (4.16 mg g^{-1}) and 2010 (4.14 mg g^{-1}). These concentrations were nearly 5 times greater than that recorded in 2006 (0.86 mg g^{-1}), the third highest dust concentration year, and more than an order of magnitude

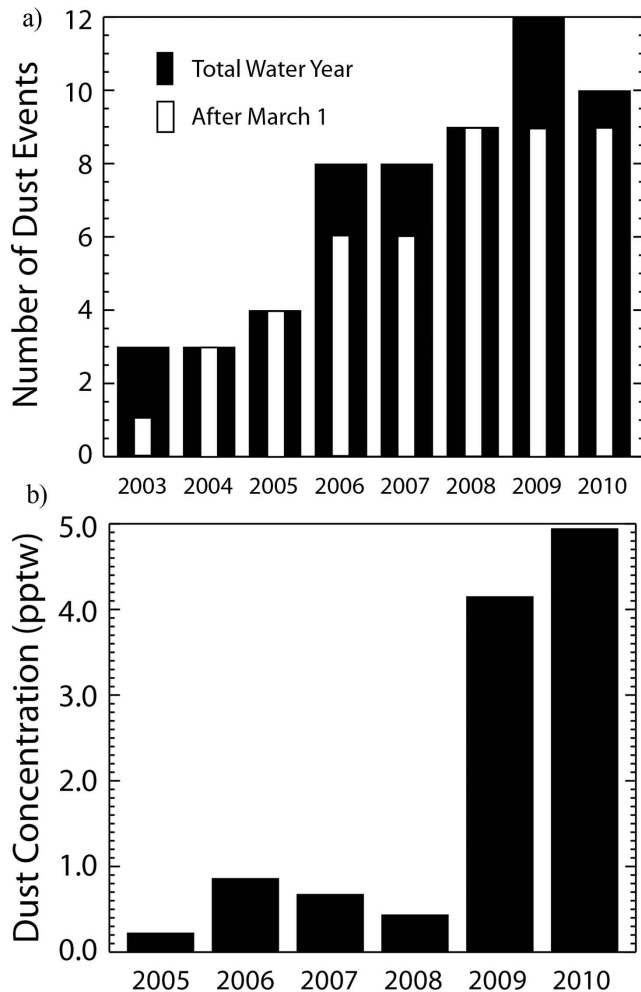


Figure 8. (a) Annual number of dust events in SBBSA in 2003–2010. (b) Annual end-of-melt season dust concentration in snowpack at the subalpine site and alpine site for 2005–2010.

greater than in 2005 (0.23 mg g^{-1}), the year with the least dust loading. Given the short period of record, it is not possible to determine whether the observed increase in dust events is part of a longer-term trend, a decadal-scale cycle, or an artifact of the observation period. As with the end of snow cover concentrations, the total dust loadings in 2009 and 2010 were by far the greatest (54.6 g m^{-2} and 45.6 g m^{-2} , respectively). In other years, dust loading ranged from 4.7 g m^{-2} to 12.7 g m^{-2} .

[26] The weekly sampling of the stratigraphy is presented as images in Figure 9 in which the vertical dimension gives the stratigraphy of the top 30 cm in 3 cm increments, and the horizontal dimension gives the approximately weekly time resolution. As noted previously, the dust concentrates on the snow surface as melt progresses, which is readily apparent in the stratigraphy time series. Spring snow events are evident, moving the high surface concentration lower in the top 30 cm layer. The increase in surface concentration with time correlates directly with the observed coincident reductions in snow surface albedo.

4.3. Meteorological and Energy Balance Measurements

[27] We show the daily meteorological data for the subalpine and alpine sites in Figure 10. Mean temperatures at the lower elevation subalpine site are most often slightly higher than those at the alpine site (Figure 10a). At the subalpine site, temperatures ranged from -24°C to 16°C with a mean annual temperature at the melting point of ice of 0°C . At the alpine site, temperatures ranged from -25°C to 15°C with a mean of -1°C .

[28] Daily mean relative humidity (RH) ranged generally from 20 to 95% with the rare excursion to as low as 10% (Figure 10b). Through most of the years, the time-integrated mean RH lies in the range 60 to 80% but begins to drop markedly in the period April/May to a minimum very near the summer solstice. At this point, the summer monsoon generally commences. The one exception to this pattern in this record was the spring of 2009 when the drying began but was quickly supplanted by a return to strong precipitation. The mean annual relative humidity at the subalpine site is 62% and for the alpine site is 58%, despite the higher temperatures at the subalpine site, possibly an effect of the surrounding forest. The difference between the two however lies within the 3% uncertainty for the RH instruments.

[29] The difference in wind speed is the most obvious difference between the meteorology at the alpine site and the subalpine site (Figure 10c). At the alpine site, the mean wind speeds were 3.7 m s^{-1} with a range of daily means of 1.1 to 11.1 m s^{-1} . At the subalpine site, the mean wind speeds were 1.1 m s^{-1} with a range of 0.3 to 3.7 m s^{-1} . Whereas wind speeds at the subalpine site have little sensitivity to season, wind at the alpine site has a strong seasonality with maximum wind speeds in winter and minimum wind speeds in July and August. The abrupt transition to lower wind speeds in summer coincides with the abrupt return of relative humidity to wintertime ranges.

[30] The global irradiance time series show that the SBBSA has relatively high irradiances due to less frequent cloud cover than in settings such as the Pacific Northwest, consistent with its characterization as a radiation-dominated continental climate (Figure 10d). Given its higher elevation and lower optical air mass, the alpine site irradiance is generally higher than that of the subalpine site. The alpine mean global irradiance was 217 W m^{-2} with a range of daily means of 43 to 424 W m^{-2} . The subalpine mean global irradiance was 205 W m^{-2} with a maximum of 403 W m^{-2} . The minima in the subalpine record are more uncertain because of the corrections described above when snow lies on the up-looking pyranometer. Whereas our calculations have minima $<20 \text{ W m}^{-2}$, we are confident that the minimum mean global irradiances lie in the range of $35\text{--}45 \text{ W m}^{-2}$. The minima in the alpine record are more reliable because higher wind speeds prevent accumulation of snow or frost.

[31] The alpine site has generally higher reflected fluxes than the subalpine because of greater global irradiance (Figure 10e) but also because it maintains a higher albedo (Figure 11). Both sites exhibit minimum reflected fluxes in summertime when vegetation is exposed. When snow cover is present, the reflected fluxes have minima near the

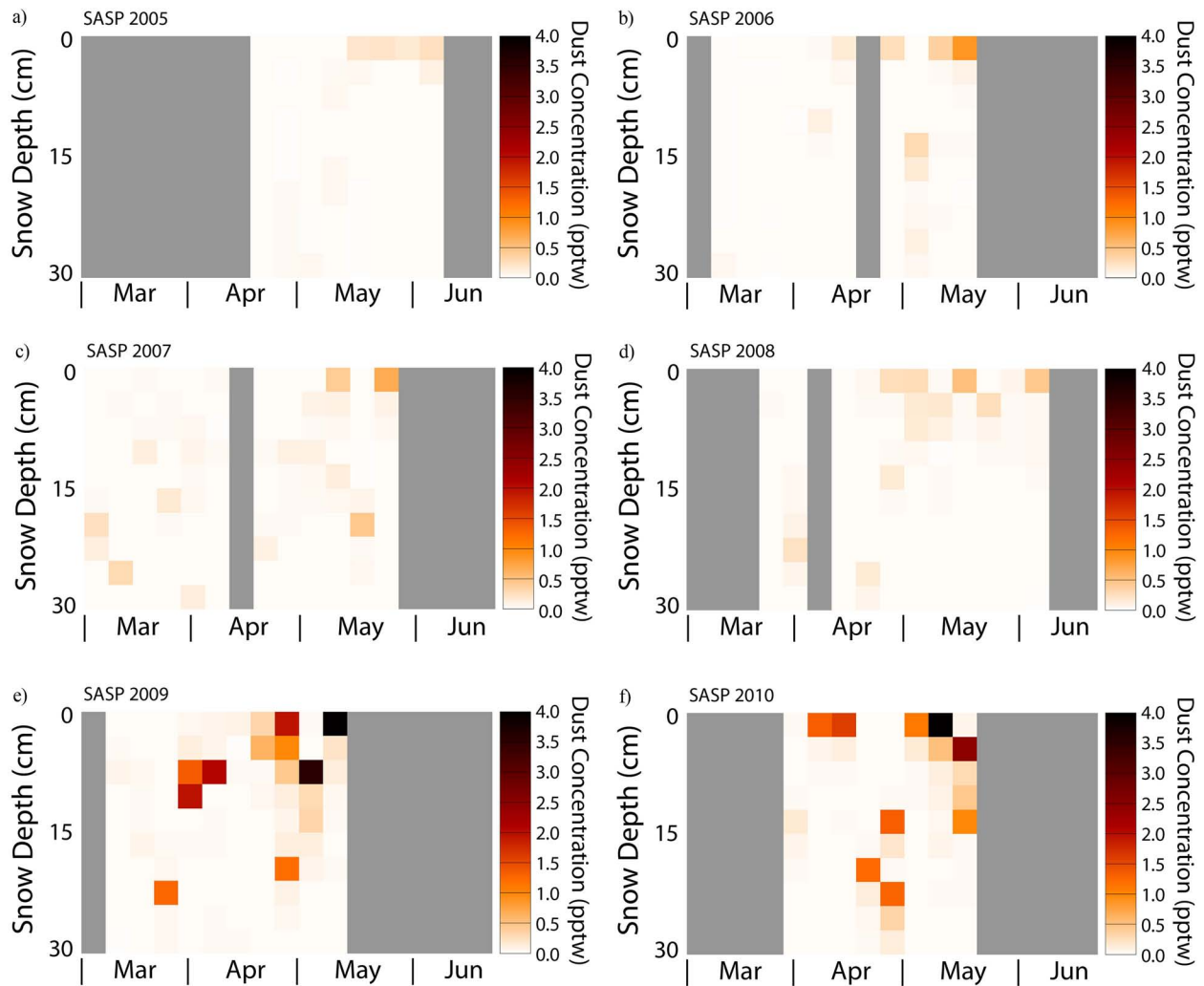


Figure 9. Image representation of the time series of dust concentrations in the top 30 cm of the snowpack at the subalpine Swamp Angel Study Plot (SASP) for 2005 through 2010. Gray columns indicate no data were collected. The continuous gray at the end indicate no snow remained.

winter solstice then rise with the global irradiance modulated by a relatively constant snow albedo until a peak that well precedes the loss of snow cover. It is during this later period that snow albedo drops due to dust radiative forcing and snow grain coarsening.

[32] Longwave irradiance is generally greater at the subalpine site due to higher temperatures, greater relative humidity, and greater air mass (Figure 10f). The larger contribution of terrain emission also increases the longwave irradiance at the subalpine site. Longwave irradiance abruptly increases in most years coincident with the increase in relative humidity and cloud cover near the summer solstice with the onset of the SW monsoon. At the subalpine site, the mean longwave irradiance was 250 W m^{-2} with minimum of 137 W m^{-2} and maximum of 344 W m^{-2} . At the alpine site, the mean longwave irradiance was 231 W m^{-2} with minimum of 118 W m^{-2} and maximum of 335 W m^{-2} . The climatology of each of these fields is presented in Figure 11.

[33] Declines in springtime broadband albedo (Figure 12) at the subalpine site generally precede those at alpine site by 1–2 weeks, due to greater wind-driven redistribution

of dust into patchy exposure in the alpine and more frequent snowfall in the late spring in the alpine. The variation in albedo comes from periodic additions of new snow during both accumulation and melt, with especially large ranges (0.3–0.9) over short time intervals in the melt season as dust layers exert their strongest influence. The climatology of broadband albedo shows relatively stable albedo (0.8–0.85) at both sites until late March after which there is a quasi-monotonic decline until mid to late May (Figure 13). The subalpine albedo drops more rapidly than the alpine albedo. Slight plateaus of albedo occur in May at ~ 0.45 in the alpine and ~ 0.35 in the subalpine before plunging to the snow-free vegetation albedo of 0.15–0.20 in June.

[34] Figure 14 shows broadband, NIR/SWIR, and visible albedo over the ablation season (15 April to snow all gone date) for the subalpine site (Figures 14a, 14c, and 14e) and alpine site (Figures 14b, 14d, and 14f). The lowest end-of-year albedos occur in 2009, the year with the highest dust concentration, greatest radiative forcing, and earliest melt out date.

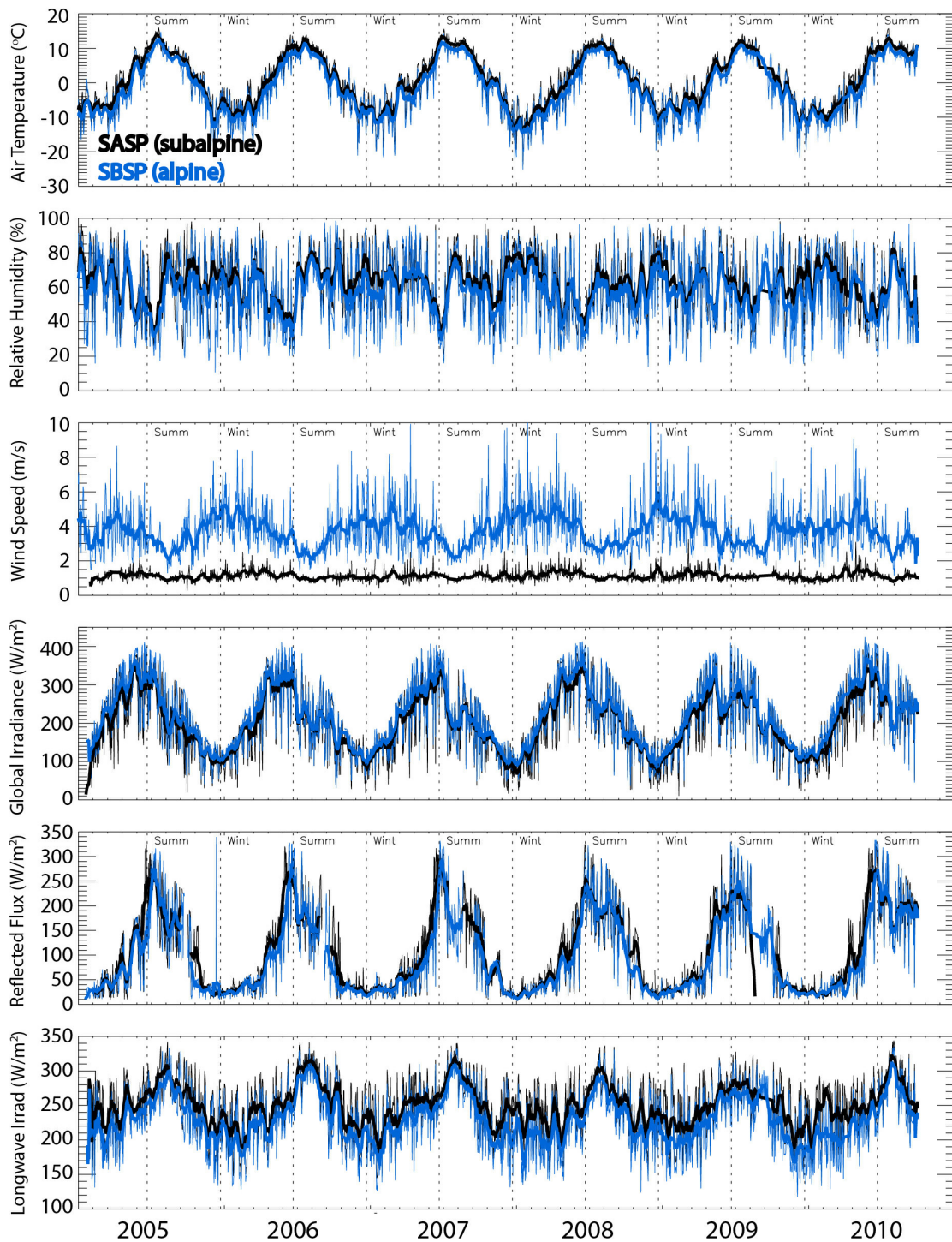


Figure 10. Time series of meteorological and radiation fields at subalpine and alpine sites for 2005 through 2010. The vertical dashed lines indicate the onset of winter (21 December) and summer (21 June). The global irradiance includes nighttime hours, so these are daily means. The year label in the abscissa axis is centered upon that calendar year's summer solstice.

[35] The decline in albedo happens relatively quickly in 2009 in comparison with the other years due to the greater radiative forcing driven by extremely high dust concentrations. There was a reduction in visible albedo from 0.72 to 0.33 over 13 days (day of year 109 to 121), more than doubling absorbed solar radiation. A precipitation event brought

the albedo back up to 0.91 at day of year 122, but it dropped again to 0.33 within 5 days (day 127) and maintained a value of about 0.3 until melt out 11 days later (day 138). The lowest average albedo over the ablation season was also observed at the subalpine site at 0.49. At the alpine site there was a similar end of year decline in albedo, which was

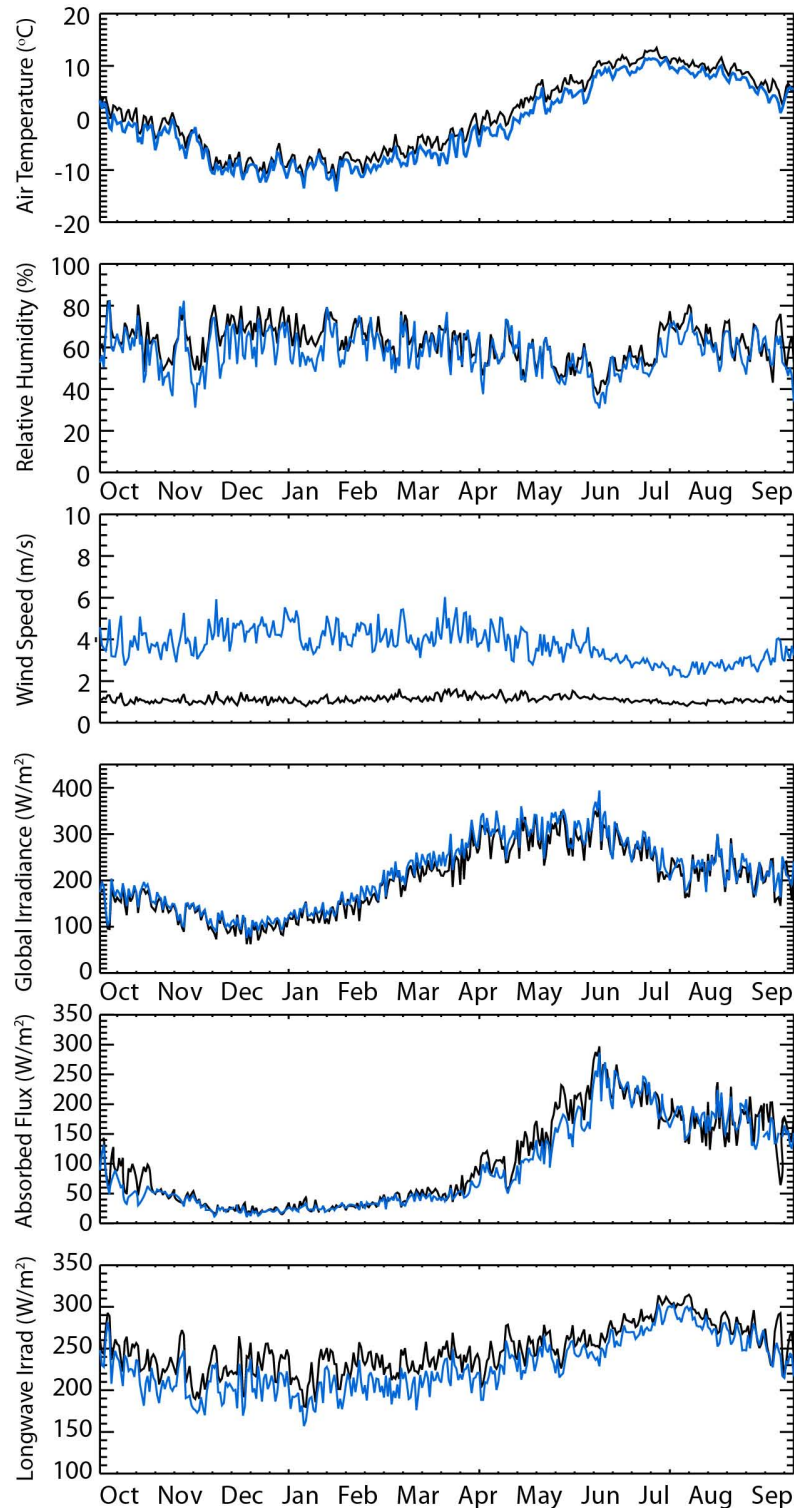


Figure 11. Daily climatologies across 2005–2010 of the meteorological and radiation fields given in Figure 10.

reduced from 0.9 at day 122 to 0.34 in 16 days (day 138) and melt out occurred within 2 days (day 140). Most literature cites snow albedo as ranging from 0.4–0.9, but 2009 and 2010 indicate values can be lower in the presence of heavy dust loading.

[36] Figure 15 shows daily snow depth and weekly snow water equivalent (SWE) for 2005 through 2010. As with other parameters, windier conditions at the alpine site cause redistribution of snow and therefore variable relationship between the snow depth measured by the sonic depth

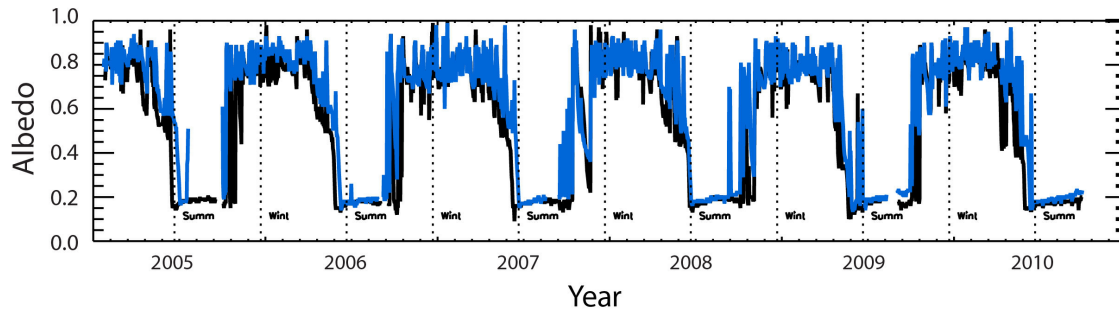


Figure 12. Time series of snow broadband albedo at subalpine and alpine sites for 2005 through 2010.

sensor on the tower and that measured in the snow pits a few meters away. However, the calmer conditions of the subalpine site allow consistency in measured snow depths at the subalpine tower and the snow pits.

[37] The magnitude of the impact of dust radiative forcing on changes in the date of snow all gone (SAG) depends on the timing and magnitude of snow accumulations before and after dust events and the total amount of snow on the ground over the melt season. For example, dust-forcing of melt of a snowpack consisting of 1 cm of SWE under average spring conditions would impact change in SAG by less than a day, whereas a 1 m snowpack allows a longer period of divergence between the dust-laden snow and a cleaner snow column subject to the same energy fluxes, resulting in multiple weeks of difference in SAG (as described in Part 2 of this paper).

[38] While there is interannual variability in snow depth and peak SWE, accumulation typically begins at the subalpine site between mid and late November and melts completely between mid May and mid June (Figure 16). Peak snow depth ranges from 2.1 m (2007) to 2.9 m (2008) with both a mean and median of 2.5 m. Peak tends to occur in mid April with the earliest peak being 27 March (2010) and latest 24 April (2007) with the mean on 11 April. At the alpine site, snow accumulation begins later (due to greater wind redistribution and scouring), typically in late November to early December, and persists between 1 day and 2 weeks later than the subalpine snowpack. Peak snow

depth ranges from 1.7 m (2009) to 2.6 m (2005) with a mean of 2.1 m and a median of 2.0 m. Peak also occurs in mid April, with the earliest peak on 7 April (2006) and latest on 24 April (2010) with mean peak occurring on 15 April.

[39] Measured peak SWE at the subalpine site ranges from 682 mm (2010) to 977 mm (2008), with a mean of 798 mm and median of 776 mm and occurs on average on 22 April (Figure 15). At the subalpine site peak SWE ranges from 575 mm (2009) to 1019 mm (2005), with a mean of 764 mm and median of 748 mm and occurs on average on 27 April. Unlike snow depth, SWE is not measured continuously so these numbers may not represent actual peak SWE. Measured SWE peaks later than snow depth discussed above, as well as being slightly higher and later than at the nearby Red Mountain Snow Telemetry (SNOTEL) site where peak SWE occurs on average on 16 April with a mean SWE of 690 mm and median of 657 mm.

[40] Over the record, the subalpine site has on average a greater snow depth and SWE than the alpine site (Figure 16). In some years, such as 2008 and 2009, lower snow depth at the alpine relative to the subalpine site is more pronounced. While the alpine site always has consistently higher winds, these years also happen to be two of the windiest over the record; the enhanced winds in these years could be contributing to lower snow depths through redistribution and densification of the alpine snowpack. Due to the small spatial extent of our measurements and the high spatial heterogeneity of snow cover in alpine environments, we consider these snow depth and SWE measurements to be representative of our sites but not necessarily the landscape.

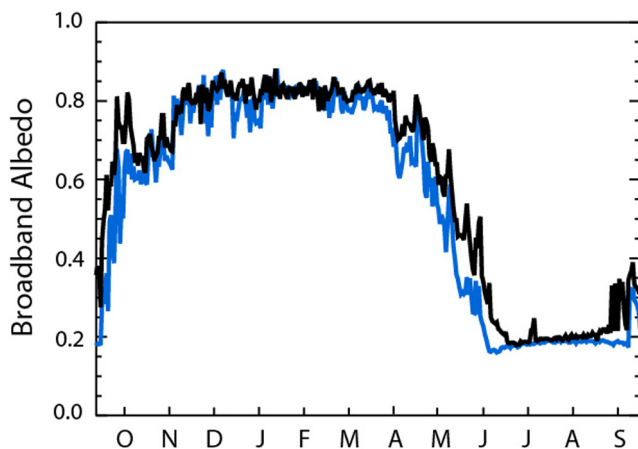


Figure 13. Daily climatology of snow albedo across 2005–2010 at subalpine and alpine sites.

5. Concluding Remarks

[41] The measurements described above are critical and unique in the Colorado River Basin. They have provided surprising insights into the controls on snowmelt and runoff in the CRB and will continue to enable monitoring and simulation of snowmelt forcings that exhibit strong interannual variability and are not captured by conventional or operational temperature index-based snowmelt models. *Painter et al.* [2007, 2010] demonstrate that dust radiative forcing of snowmelt has dramatic impacts on snowmelt timing, melt-out date, and hydrology across the Upper Colorado River Basin, with important ramifications for water management, planning, and policy.

[42] *Munson et al.* [2011] suggest that dust deposition on Colorado River snow stands to increase with regional warming. Therefore, it is possible that the heavy dust

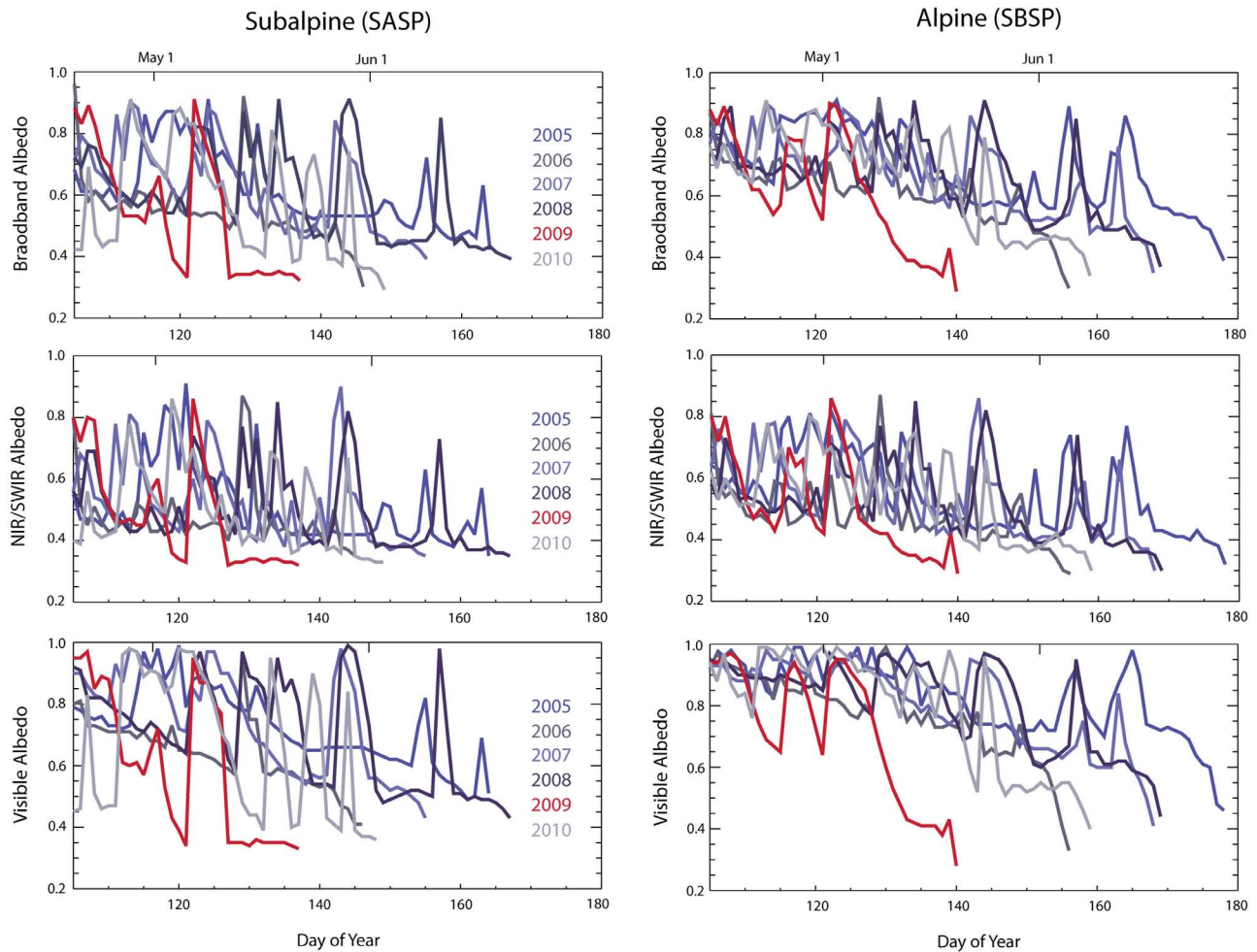


Figure 14. Time series of snowmelt season broadband, near-infrared/shortwave infrared (NIR/SWIR), and visible albedo by year for 2005–2010.

depositions observed in 2009 and 2010 represent the future normal condition. Many studies indicate that climate warming will strongly impact Colorado River flows [Christensen and Lettenmaier, 2007; Barnett and Pierce, 2009; Hurkmans et al., 2009], as temperature increases change rain/snow

proportions, the length of the snow season, and potential evapotranspiration. Recent bark beetle epidemics and associated forest management responses threaten to alter the hydrologic response of headwater catchments to diurnal and seasonal snowmelt cycles.

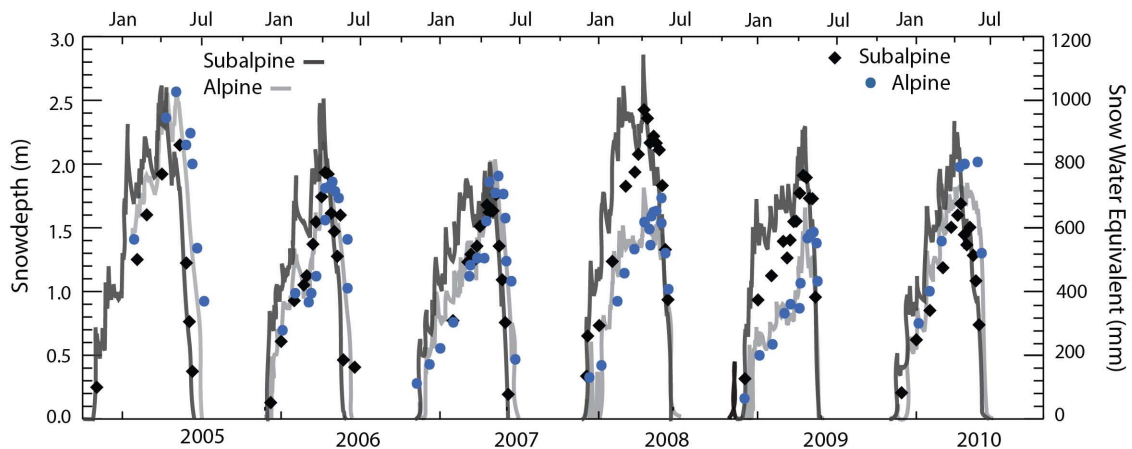


Figure 15. Time series of snow depth and snow water equivalent by year for 2005–2010.

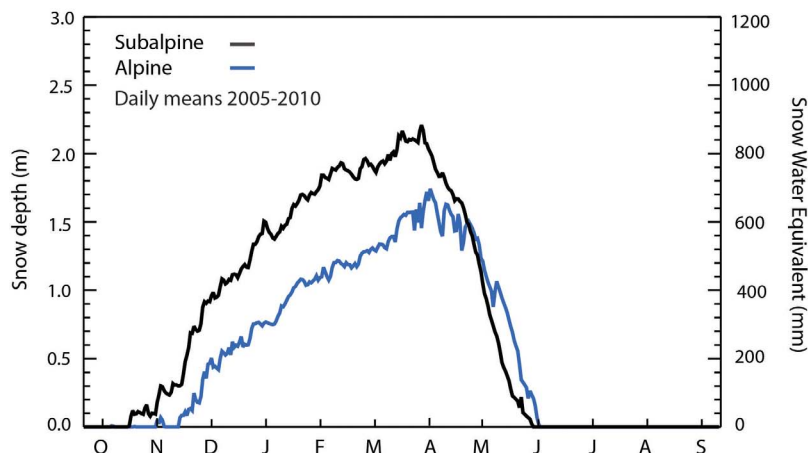


Figure 16. Daily climatology of snow depth across 2005–2010. We do not include climatology of SWE because of the sparse and out-of-phase nature of sampling.

[43] Analyses of snow accumulation and melt forcing under dust, climate warming, or vegetation change scenarios are not possible without the type of measurements detailed here—in fact, the far-reaching ramifications of the measurements and results described above, in the companion paper, and in the reference for Painter *et al.* [2007, 2010] demand an expanded capacity to conduct direct monitoring of snow energy balance throughout the Upper Colorado River Basin and other snowmelt-dominated basins in the Western United States.

[44] **Acknowledgments.** This work was funded by the National Science Foundation grants ATM04323237 and ATM0431955, and NASA project NNX10AO97G. We acknowledge the assistance of Andrew Barrett in data processing. Part of this work was performed at the Jet Propulsion Laboratory, California Institute of Technology under a contract with NASA. We thank Jeff Dozier, Steve Warren, and an anonymous reviewer for their suggestions that improved this manuscript.

References

- Ajai, L., et al. (2011), *Fate of Mountain Glaciers in the Anthropocene*, 15 pp., Pontifical Acad. of Sci., Vatican City.
- Bales, R. C., N. P. Molotch, T. H. Painter, M. D. Dettinger, R. Rice, and J. Dozier (2006), Mountain hydrology of the Western United States, *Water Resour. Res.*, *42*, W08432, doi:10.1029/2005WR004387.
- Barnett, T. P., and D. W. Pierce (2009), Sustainable water deliveries from the Colorado River in a changing climate, *Proc. Natl. Acad. Sci. U. S. A.*, *106*, 7334–7338, doi:10.1073/pnas.0812762106.
- Christensen, N. S., and D. P. Lettenmaier (2007), A multimodel ensemble approach to assessment of climate change impacts on the hydrology and water resources of the Colorado River Basin, *Hydrol. Earth Syst. Sci.*, *11*, 1417–1434, doi:10.5194/hess-11-1417-2007.
- Conway, H., A. Gades, and C. F. Raymond (1996), Albedo of dirty snow during conditions of melt, *Water Resour. Res.*, *32*, 1713–1718, doi:10.1029/96WR00712.
- Higuchi, K., and A. Nagoshi (1977), Effect of particulate matter in surface snow layers on the albedo of perennial snow patches, in *Isotopes and Impurities in Snow and Ice*, edited by J. F. Nye, F. Miller and H. Oeschger, IAHS AISH Publ., 118, 95–97.
- Hurkmans, R., P. A. Troch, R. Uijlenhoet, P. Torfs, and M. Durcik (2009), Effects of climate variability on water storage in the Colorado River Basin, *J. Hydrometeorol.*, *10*, 1257–1270, doi:10.1175/2009JHM1133.1.
- Jonsell, U., R. Hock, and B. Holmgren (2003), Spatial and temporal variations in albedo on Storglaciaren, Sweden, *J. Glaciol.*, *49*, 59–68, doi:10.3189/172756503781830980.
- Kaspari, S., P. A. Mayewski, M. Handley, S. Kang, S. Hou, S. Sneed, K. Maasch, and D. Qin (2009), A high-resolution record of atmospheric dust composition and variability since A.D. 1650 from a Mount Everest ice core, *J. Clim.*, *22*, 3910–3925, doi:10.1175/2009JCLI2518.1.
- Lawrence, C. R., T. H. Painter, and J. C. Neff (2010), Contemporary geochemical composition and flux of aeolian dust to the San Juan Mountains, Colorado, United States, *J. Geophys. Res.*, *115*, G03007, doi:10.1029/2009JG001077.
- MacDonald, G. M. (2010), Water, climate change, and sustainability in the southwest, *Proc. Natl. Acad. Sci. U. S. A.*, *107*, 21,256–21,262, doi:10.1072/pnas.0909651107.
- Munson, S. M., J. Belnap, and G. S. Okin (2011), Responses of wind erosion to climate-induced vegetation changes on the Colorado Plateau, *Proc. Natl. Acad. Sci. U. S. A.*, *108*, 3854–3859, doi:10.1073/pnas.1014947108.
- Neff, J. C., A. P. Ballantyne, G. L. Farmer, N. M. Mahowald, J. L. Conroy, C. C. Landry, J. T. Overpeck, T. H. Painter, C. R. Lawrence, and R. L. Reynolds (2008), Increasing eolian dust deposition in the western United States linked to human activity, *Nat. Geosci.*, *1*, 189–195, doi:10.1038/ngeo133.
- Oerlemans, J. (2000), Analysis of a 3 year meteorological record from the ablation zone of Morteratschgletscher, Switzerland: Energy and mass balance, *J. Glaciol.*, *46*, 571–579, doi:10.3189/172756500781832657.
- Painter, T. H., A. P. Barrett, C. C. Landry, J. C. Neff, M. P. Cassidy, C. R. Lawrence, K. E. McBride, and G. L. Farmer (2007), Impact of disturbed desert soils on duration of mountain snow cover, *Geophys. Res. Lett.*, *34*, L12502, doi:10.1029/2007GL030284.
- Painter, T. H., J. S. Deems, J. Belnap, A. F. Hamlet, C. C. Landry, and B. Udall (2010), Response of Colorado River runoff to dust radiative forcing in snow, *Proc. Natl. Acad. Sci. U. S. A.*, *107*, 17,125–17,130, doi:10.1073/pnas.0913139107.
- Ramanathan, V., M. V. Ramana, G. Roberts, D. Kim, C. Corrigan, C. Chung, and D. Winker (2007), Warming trends in Asia amplified by brown cloud solar absorption, *Nature*, *448*, 575–578, doi:10.1038/nature06019.
- Skiles, S. M., T. H. Painter, J. S. Deems, A. C. Bryant, and C. Landry (2012), Dust radiative forcing in snow of the Upper Colorado River Basin: Part II. Interannual variability in radiative forcing and snowmelt rates, *Water Resour. Res.*, doi:10.1029/2012WR011986, in press.
- United Nations Environmental Programme/World Meteorological Organization (2011), *Integrated assessment of black carbon and tropospheric ozone*, 285 pp., U. N. Environ. Prog., Nairobi, Kenya.

Dust radiative forcing in snow of the Upper Colorado River Basin: 2. Interannual variability in radiative forcing and snowmelt rates

S. McKenzie Skiles,^{1,2} Thomas H. Painter,^{1,2,3} Jeffrey S. Deems,^{4,5} Ann C. Bryant,⁶ and Christopher C. Landry⁷

Received 27 February 2012; revised 25 May 2012; accepted 7 June 2012; published 26 July 2012.

[1] Here we present the radiative and snowmelt impacts of dust deposition to snow cover using a 6-year energy balance record (2005–2010) at alpine and subalpine micrometeorological towers in the Senator Beck Basin Study Area (SBBSA) in southwestern Colorado, USA. These results follow from the measurements described in part I. We simulate the evolution of snow water equivalent at each station under scenarios of observed and dust-free conditions, and +2°C and +4°C melt-season temperature perturbations to these scenarios. Over the 6 years of record, daily mean dust radiative forcing ranged from 0 to 214 W m⁻², with hourly peaks up to 409 W m⁻². Mean springtime dust radiative forcings across the period ranged from 31 to 49 W m⁻² at the alpine site and 45 to 75 W m⁻² at the subalpine site, in turn shortening snow cover duration by 21 to 51 days. The dust-advanced loss of snow cover (days) is linearly related to total dust concentration at the end of snow cover, despite temporal variability in dust exposure and solar irradiance. Under clean snow conditions, the temperature increases shorten snow cover by 5–18 days, whereas in the presence of dust they only shorten snow duration by 0–6 days. Dust radiative forcing also causes faster and earlier peak snowmelt outflow with daily mean snowpack outflow doubling under the heaviest dust conditions. On average, snow cover at the towers is lost 2.5 days after peak outflow in dusty conditions, and 1–2 weeks after peak outflow in clean conditions.

Citation: Skiles, S. M., T. H. Painter, J. S. Deems, A. C. Bryant, and C. C. Landry (2012), Dust radiative forcing in snow of the Upper Colorado River Basin: 2. Interannual variability in radiative forcing and snowmelt rates, *Water Resour. Res.*, 48, W07522, doi:10.1029/2012WR011986.

1. Introduction

[2] In part I of this paper [Painter *et al.*, 2012] we present the detailed energy balance measurements required for investigation of radiative impacts of desert dust in alpine and subalpine snow cover, using data collected at the Senator Beck Basin Study Area (SBBSA) in the San Juan Mountains of southwest Colorado. Previously, Painter *et al.* [2007] isolated the effects of dust from other controls and showed with a two-year data set that the acceleration of melt by the shortwave

radiative forcing of dust results in a shortening of snow cover duration in southwest Colorado by 18–35 days. In the present study we expand on Painter *et al.* [2007] to encompass the full observation period at our study sites, from 2005 through 2010. Additionally, given that by 2050 temperature increases of 2°C–4°C are projected in this region [Barnett and Pierce, 2009], we model the sensitivity of snowmelt to increases in melt season temperature by which to understand the relative magnitudes of forcings by dust and atmospheric warming, separately and in combination.

¹Department of Geography, University of California, Los Angeles, California, USA.

²Joint Institute for Regional Earth System Science and Engineering, University of California, Los Angeles, California, USA.

³Jet Propulsion Laboratory, California Institute of Technology, Pasadena, California, USA.

⁴National Snow and Ice Data Center, Boulder, Colorado, USA.

⁵NOAA Western Water Assessment, Boulder, Colorado, USA.

⁶Department of Geography, University of Utah, Salt Lake City, Utah, USA.

⁷Center for Snow and Avalanche Studies, Silverton, Colorado, USA.

Corresponding author: T. H. Painter, Jet Propulsion Laboratory, California Institute of Technology, 4800 Oak Grove Dr., Pasadena, CA 91109, USA. (thomas.painter@jpl.nasa.gov)

2. Methods

2.1. Radiative Forcing

[3] Radiative forcing by dust in snow directly affects the snowpack through enhanced absorption of solar radiation by dust (direct effect), and indirectly through enhanced absorption by larger grain size due to acceleration of grain growth from the direct effect (first indirect effect) and by the earlier exposure of a darker substrate (second indirect effect) [Hansen and Nazarenko, 2004]. From the micrometeorological measurements discussed in part I of this paper, the range of dust radiative forcings is determined using the treatment described by Painter *et al.* [2007].

[4] We calculate minimum and maximum radiative forcing to account for the range of potential radiative forcing

due to dust. Minimum surface radiative forcing addresses the direct effect of dust in snow by accounting for the reduction of snow albedo in the visible wavelengths. The maximum radiative forcing includes both the direct effect and the first indirect effect (*i1*) by accounting for reduction in visible albedo due to dust and reductions in the near infrared/shortwave infrared (NIR/SWIR) albedo from increases in grain size. The maximum forcing also includes direct forcing from perturbation of snow albedo in the NIR [Singh *et al.*, 2010; Painter, 2011].

[5] Minimum surface radiative forcing f_{dmin} (W m^{-2}) is calculated as

$$F_{dmin} = E_{vis}\Delta_{vis}, \quad (1)$$

where E_{vis} is the visible irradiance (W m^{-2}) determined from the difference between the broadband and NIR/SWIR irradiances, $\Delta_{vis} = 0.92 - a_{vis}$, a_{vis} is calculated visible albedo, and 0.92 is the observed mean visible albedo for relatively dust-free snow at our study sites (no midlatitude snow is completely free of aerosols) [Painter *et al.*, 2007].

[6] Maximum surface radiative forcing F_{dmax+1} is calculated as

$$F_{dmax+1} = 0.5[E_{vis}\Delta_{vis} + E_{NIR/NIR}(1/\xi) - 1], \quad (2)$$

where

$$\xi = 1 - 1.689\Delta_{vis}\Delta_{vis} \leq 0.17,$$

$$\xi = 0.67\Delta_{vis} > 0.17,$$

E_{NIR} is the NIR/SWIR net shortwave flux, and a_{NIR} is the NIR/SWIR albedo. The latter empirical relationship was developed in SBBSA and gives the proportion of the change in NIR/SWIR albedo due to the presence of dust versus grain coarsening in the absence of dust [Marks *et al.*, 1998; Painter *et al.*, 2007].

2.2. Temperature Change

[7] The relative capacities of radiative forcing by dust and temperature increases to accelerate snowmelt are addressed by simulating snowmelt with uniform, hourly temperature perturbations of $+2^\circ\text{C}$ and $+4^\circ\text{C}$ during the melt season, with and without dust. An increase in temperature increases sensible heating and longwave irradiance to the snow surface. The change in sensible heating is directly related to the temperature increase, whereas the increase in longwave irradiance depends also on the fraction of sky that is cloud covered and the relative humidity (which in turn affect the atmospheric emissivity). Cloud cover fraction is a difficult variable to estimate, so we bracket increases in longwave irradiance with treatments of clear sky and complete cloud conditions.

[8] Perturbations to the clear sky longwave irradiance are calculated with the parameterization described by Konzelmann *et al.* [1994]:

$$L = [0.23 + 0.443(e_a/T_a)^{1/8}](\sigma T_a^4), \quad (3)$$

where e_a is vapor pressure (Pa), T_a is air temperature (K), and σ is the Stefan-Boltzmann constant ($5.67 \times 10^{-8} \text{ W m}^{-2} \text{ K}^{-4}$). This represents the Stefan-Boltzmann

equation where $0.23 + 0.443(e_a/T_a)^{1/8}$ is the clear sky emissivity, with 0.23 being emissivity under a completely dry atmosphere.

[9] Longwave irradiance from a completely cloud covered sky is primarily determined by the temperature of the cloud base. We determine the perturbation of longwave under cloud cover with the following relation [Konzelmann *et al.*, 1994]:

$$L = \{[0.23 + 0.443(e_a/T_a)^{1/8}](1 - n^3) + 0.963n^3\}\sigma T_a^4, \quad (4)$$

where n is the fractional cloud cover and all others are as above. When the cloud cover is treated as complete, $n = 1$, the relation collapses to

$$L = (0.963)\sigma T_a^4, \quad (5)$$

where 0.963 is the emissivity under complete cloud cover. The ideal longwave parameterization would utilize data at our sites, a relationship we are currently working on developing. Until then we use these physically based relations which were developed in Greenland but have also been shown to perform well in a glacier environment in northern Sweden [Sedlar and Hock, 2009].

2.3. Snowmelt Model

[10] We use the point snow energy balance model (SNOBAL) to calculate snowmelt and predict point runoff using SBBSA tower and snow plot data on snow properties, measurement heights and depths, and energy exchanges [Marks and Dozier, 1992; Marks *et al.*, 1992]. In the model, the snowpack is represented as two layers: a 25 cm surface layer where energy exchanges take place, and the remainder of the pack as an energy and mass storage layer. The model utilizes site elevation, measurement heights, roughness length, and initial snow state variables (snow depth, snow density, snow surface temperature, average snowpack temperature, and liquid water content) as starting inputs. Snow variables and measurement heights are then updated at each time step (Figure 1). Energy exchanges are calculated in the active upper layer and then energy transfer is determined for the snowpack as a whole, from which the energy available for phase changes in both layers is determined. Melt is computed once the cold content (energy required to bring the temperature of the snow to 0°C) reaches 0 J m^{-2} . The cold content (Q) is calculated using the following equation:

$$Q = \rho h c_s (T_0 - T^n), \quad (6)$$

where ρ is the snow density, h is the snow height, c_s is the specific heat of ice, T_0 is melting temperature (0°C or 273.15 K), and T^n is the snow temperature (in either $^\circ\text{C}$ or K , depending on units for melting temperature) [Marks *et al.*, 1998]. When the liquid water content in the snowpack exceeds the amount allowed by the maximum liquid water holding capacity, the ratio of the volume of water with the difference between the volume of snow and volume of ice, then evaporation and snowpack outflow are estimated from the lower layer [Marks *et al.*, 1998].

[11] For this study we ran the model over the springtime melt season. The starting snowpack conditions, or state

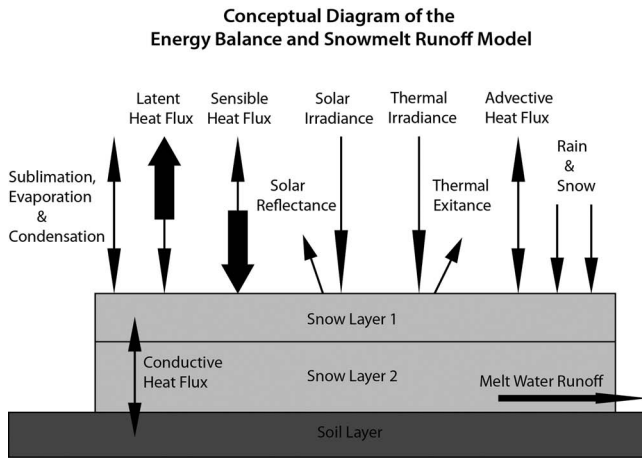


Figure 1. Conceptual diagram of SNOBAL model structure and components (after Marks et al. [1998]).

variables mentioned above, were determined from the manual snow measurements performed closest in time to 15 April (the date of average peak snow for the region) at each site. Changes in state variables, updated at an hourly time step, are driven by the observed forcing variables (hourly averages of net shortwave, longwave irradiance, air temperature, relative humidity, and wind speed), which are measured at the micrometeorological towers as described in part I of this paper (state and forcing variables summarized in Table 1). Soil temperature is set to 0°C for the model runs because the snow soil temperature is generally at or near 0°C in our observations and its flux to the snowpack is considered to have a negligible energy contribution [Marks and Dozier, 1992]. The model is used to predict snowmelt for 15 combinations of dust and temperature scenarios (Table 2). To simplify the presentation of our results we reduce the 15 sets of outputs to a set of six scenarios: observed conditions (D_0), observed conditions with dust radiative forcings removed (C_0), and each of these scenarios with the 2°C (D_2 , C_2) and 4°C (D_4 , C_4) temperature increases.

2.4. Sensitivity and Uncertainty

[12] SNOBAL has been shown to reproduce measured snowpack properties well [Marks et al., 1998; Painter et al., 2007], however measurement uncertainty and assumptions made in calculating energy flux in the model are unavoidable. We address the uncertainties for the tower instruments and the model sensitivity to parameter uncertainties by perturbing the values of each of the input parameters to the

Table 1. SNOBAL Forcing Variables and Modeled State Variables (After Marks et al. [1998])

State Variables	Forcing Variables
Snow depth (m)	Net solar radiation ($W m^{-2}$)
Snow density ($kg m^{-3}$)	Incoming longwave radiation ($W m^{-2}$)
Snow surface layer temperature (°C)	Air temperature (°C)
Average surface layer temperature (°C)	Vapor pressure (Pa)
Average snow liquid water content (%)	Wind speed ($m s^{-1}$)

Table 2. SNOBAL Is Run for All Scenarios Shown in the First Column; the Scenario Results Shown in the Second Column are Scenario Means in Every Case But the Observed (D_0) Scenario

SNOBAL Scenarios	Results Scenarios
Dust (Observed)	D_0
Clean, maximum RF	
Clean, minimum RF	C_0
Dust +2°C, clear skies	
Dust +2°C, cloudy skies	D_2
Dust +4°C, clear skies	
Dust +4°C, cloudy skies	D_4
Clean Max +2°C, clear skies	
Clean Max +2°C, cloudy skies	
Clean Min +2°C, clear skies	
Clean Min +2°C, cloudy skies	C_2
Clean Max +4°C, clear skies	
Clean Max +4°C, cloudy skies	
Clean Min +4°C, clear skies	
Clean Min +4°C, cloudy skies	C_4

ranges in instrument uncertainty at the subalpine tower over the 2007 ablation season.

[13] Movement of air near the snow surface is influenced by surface roughness, which in turn influences turbulent exchange energy transfer. Snow surface roughness is not constant and varies at different scales, both spatial and temporal [Brock et al., 2006; Fassnacht et al., 2009]. Published roughness lengths for snow include 0.2 mm for fresh snow [Poggi, 1976], average of 1.9 mm for annual snow cover [Pluss and Mazzoni, 1994], and 1–12 mm for rough snow [Jackson and Carroll, 1978]. While dust in snow can have varying impacts on surface roughness, Fassnacht et al. [2009] found that deposited dust melts snow more uniformly, which decreases roughness relative to surrounding cleaner snow surfaces. Rhodes et al. [1987] also found this would be the case in areas where solar radiation dominates energy balance following Ball’s normal trajectory theory [Ball, 1954].

[14] For this analysis surface roughness was altered from the default 1 mm value to 5 mm, 1 cm, and 5 cm to test the sensitivity of the model to this parameter. The high value of 5 cm is used only to assess the model sensitivity; a surface roughness of 5 cm at the study plots is highly unlikely given typically observed surface roughness for alpine snow cover and at our study plots, though this could be achieved in areas of large suncup development.

3. Results

3.1. Radiative Forcing

[15] We calculated maximum and minimum radiative forcing (RF) due to dust in snow from 15 March to the date of modeled clean snow-all-gone date (SAG), as described above. While snowpack cold content is consistently nonzero during the period 15 March to 15 April, dust radiative forcing tends to begin during this period. The average of the two RF scenarios is plotted as daily means along with dust events, observed precipitation, and snow depth (Figure 2). RF is typically lower at the alpine site where dust concentrations tend to be lower and albedo higher. Remote sensing analyses suggest that the alpine tower is situated in an area of lower dust concentrations relative to most of the surrounding alpine

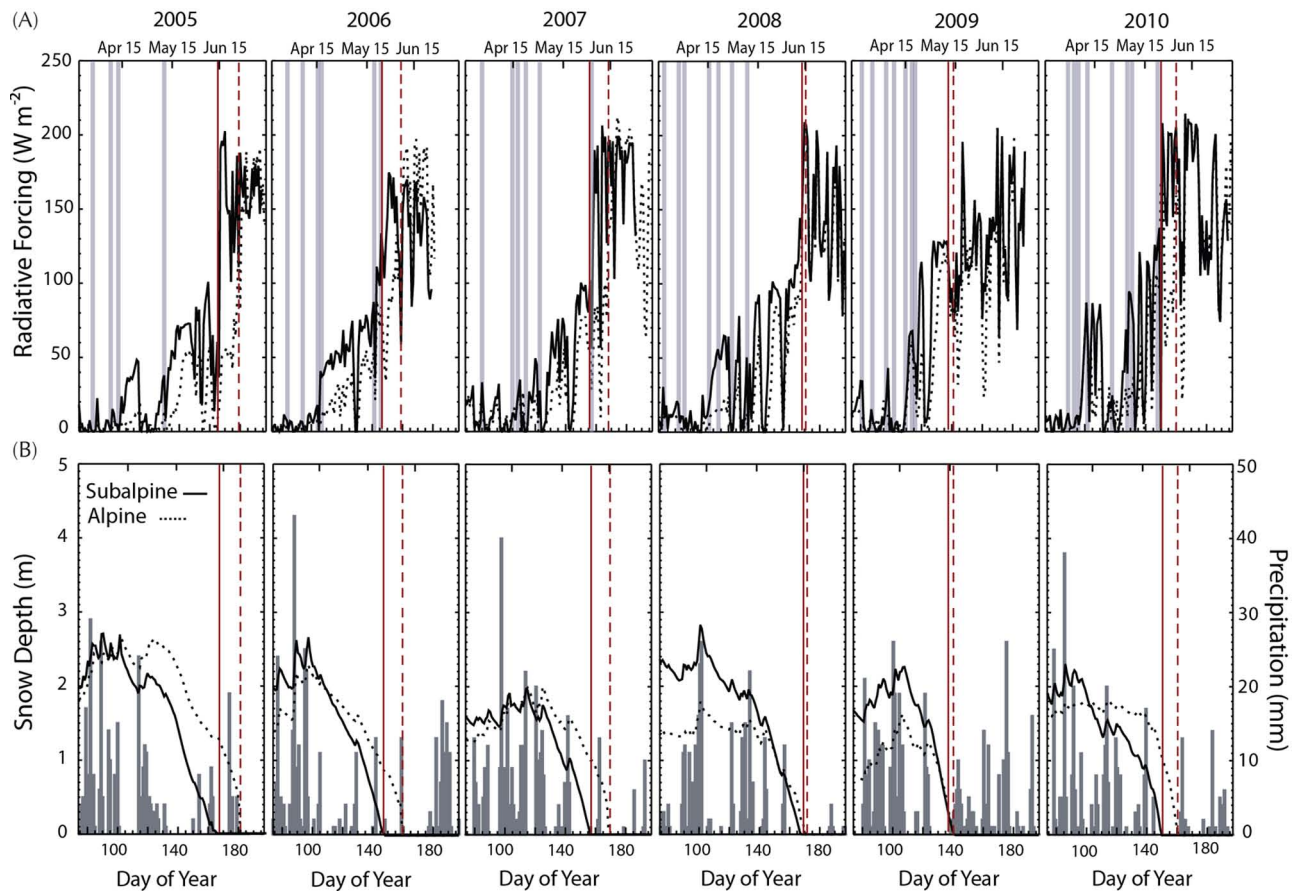


Figure 2. Time series of daily mean (a) dust radiative forcing, precipitation, and (b) snow depth at the subalpine (solid) and alpine (dashed) site from 15 March. Gray bars indicate a dust event and red bars indicate observed date of snow all gone (SAG) at each site.

terrain. This is most likely due to wind redistribution at this particularly windy site.

[16] RF varies on multiple temporal scales but typically increases after a dust event and decreases with a new snow precipitation event. Some dust events are accompanied by snowfall. In these cases the cleaner overlying new snow delays or reduces radiative forcing until the snow melts to a sufficiently low optical thickness that irradiance can interact with the dust layer. As the season advances, RF increases steadily as snow melts and previously buried dust layers converge at the snow surface.

[17] The year with the highest end of year dust concentration, 2009, also had the highest average mean daily RF over the ablation season, from 15 April to observed SAG, at 75 W m^{-2} at the subalpine site. This is a further 15 W m^{-2} over the next highest dust concentration year, 2010, and an additional 30 W m^{-2} over the lowest dust concentration year, 2005, which still had average RF of 45 W m^{-2} . The corresponding numbers at the alpine site are 50 W m^{-2} in 2009, an additional 7 W m^{-2} over 2010, and 33 W m^{-2} over 2005.

[18] Mean daily RF over the period from observed SAG (D_0) to modeled clean SAG (C_0) provides a measure of the contribution of the second indirect effect because the time between D_0 SAG and modeled C_0 SAG is when there would still be snow cover in the absence of dust. The RF varies

over this period from 136 W m^{-2} (2006) to 150 W m^{-2} (2005), with an average of 144 W m^{-2} . Mean daily RF from 15 April to C_0 SAG, then, provides a measure of all effects, direct and both indirect effects. The daily mean RF over this period is again highest in 2009 with 114 W m^{-2} at the subalpine site and 84 W m^{-2} at the alpine site, for 2010, equivalent numbers of 100 and 81 W m^{-2} , and for 2005, 79 and 56 W m^{-2} . In all cases there is an additional $30\text{--}40 \text{ W m}^{-2}$ of radiative forcing for the period of 15 April to C_0 SAG relative to D_0 SAG, this contribution coming from the time period when the snow is no longer on the ground, but would be in the absence of dust. The influence of this enhanced absorption on snow cover duration and melt is discussed below.

[19] In addition to variation in dust loading, variation in cloud cover, which impacts amount of incoming solar radiation, and new precipitation, which impacts the amount of time dust is exposed at the surface, over each spring season modulates calculated RF values (Figure 3). Springtime cumulative broadband irradiance, the total incoming solar radiation over the spring season between 15 April and 1 June, indicates interannual variability due to cloud cover. Over the whole record, changes in solar irradiance do not explain the difference in RF between high and low dust concentration years. For example, 2009 was a relatively cloudy spring with the lowest cumulative irradiance yet has the highest average springtime RF (Figure 3b).

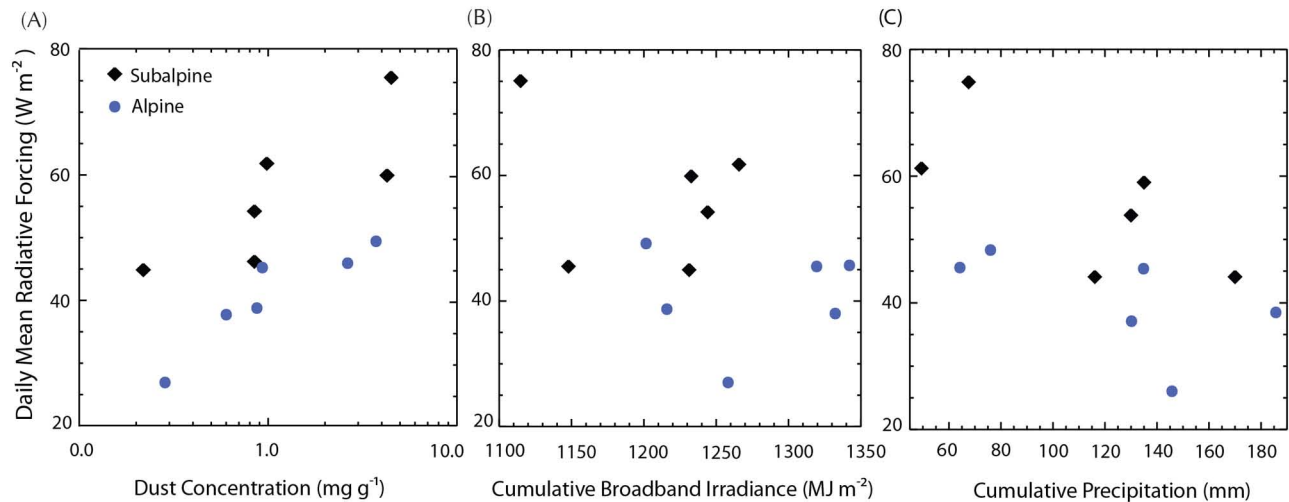


Figure 3. Daily mean radiative forcing with (a) end of year dust concentrations, (b) cumulative spring-time broadband irradiance, and (c) cumulative springtime precipitation.

[20] New snowfall during the springtime season (15 April to D_0 SAG) dampens RF by increasing the snow albedo and temporarily isolating/reducing the interaction of irradiance with the dust layer. Daily mean RF shows a weakly negative relationship with cumulative springtime precipitation (Figure 3c). The combination of the three plots indicates that variable spring conditions do impact interannual variability in RF, with the majority of the variation due to total dust loading but modulated by springtime precipitation.

3.2. Longwave Irradiance and Turbulent Exchange

[21] Subalpine observed and modeled longwave irradiances are plotted (Figure 4) for increased temperature scenarios along with modeled sensible and latent heat fluxes for the D_0 , D_2 , and D_4 scenarios. The data from the alpine site (not shown) are very similar. Comparing Figure 4 with Figure 2 gives an indication of the magnitude of changes in fluxes due to temperature increase versus dust radiative forcing. Consistently across all years (2005–2010) and at both sites temperature increases of 2°C and 4°C increase daily mean longwave irradiance by averages of 8 and 16 $W m^{-2}$, respectively, and increase daily mean sensible heating by about 2 and 4 $W m^{-2}$, respectively. The impact on latent heat transfer is negligible, varying between $\pm 1 W m^{-2}$ over all years. In comparison, in high dust concentration years enhanced surface shortwave absorption due to dust can be as high as 75 $W m^{-2}$ (2009, subalpine site), and even in the lowest dust concentration year, 2005, dust enhanced shortwave absorption by 27 to 45 $W m^{-2}$ (alpine, subalpine).

3.3. Model Accuracy

[22] We assess the SNOBAL accuracy according to its simulation of SAG and the time series of snow water equivalent relative to observations. For years 2005 through 2010, modeled SAG occurred within 1 day of observed SAG at both sites with the exception of the alpine site in 2005, when it was 2 days. This greater error resulted from inaccurate partitioning of precipitation phase during a rain on snow event at the end of the snow cover season.

[23] Measured SWE is closest to modeled SWE at the subalpine site, with a RMSE of 68 mm over all years (Figure 7).

The difference between measured and modeled SWE was higher at the alpine site, with an RMSE of 119 mm over all years. The greater differences at the alpine site occur because snow depth has been observed to be consistently deeper in the snow pit plot than at the tower several meters away [Painter *et al.*, 2012]. The snow pit depths are greater by a mean of 20 cm (median 21 cm) and standard deviation of 7 cm over all years. If SWE is calculated using depth at the tower and mean pit density the result over all years is a mean difference of 90 mm. We use tower depth to calculate the plotted alpine SWE_m numbers (Figure 7) because we consider this to be more representative of the snowpack at the tower where the energy balance and radiation measurements are made. The magnitude of the variation could potentially induce uncertainties in the model results because the model is initiated with measurements from the snow pits, but forced with data measured at the tower.

3.4. Sensitivity and Uncertainty

[24] We modeled melt season SWE evolution for all individual parameters and their respective ranges in accuracy (Figure 5a). Individually, the greatest sensitivity of 2 days difference in SAG (ΔSAG) by the end of season occurred with the longwave irradiance, which has an instrument uncertainty of $\pm 3\%$. The next largest change occurred for net solar radiation and wind with almost a 1-day difference for each parameter. The sensitivities for air temperature, vapor pressure, and precipitation were negligible. SWE for all parameters accuracy ranges (Figure 5b) represents the maximum uncertainty involved with instrument measurements, which is 2 days ΔSAG for the maximum uncertainty range (+) and 3 days difference in SAG for the minimum uncertainty range (-).

[25] We plot the average ΔSAG with simulated changes in surface roughness at the subalpine and alpine sites (Figure 6). Due to model turbulent flux parameters snowmelt could not be simulated with a 5 cm surface roughness given the low wind speeds recorded at the subalpine site. For surface roughness of 5 mm in the dust case at both sites melt is either not impacted (subalpine), or advanced by 1 day (alpine). The largest difference in melt-out occurs for the

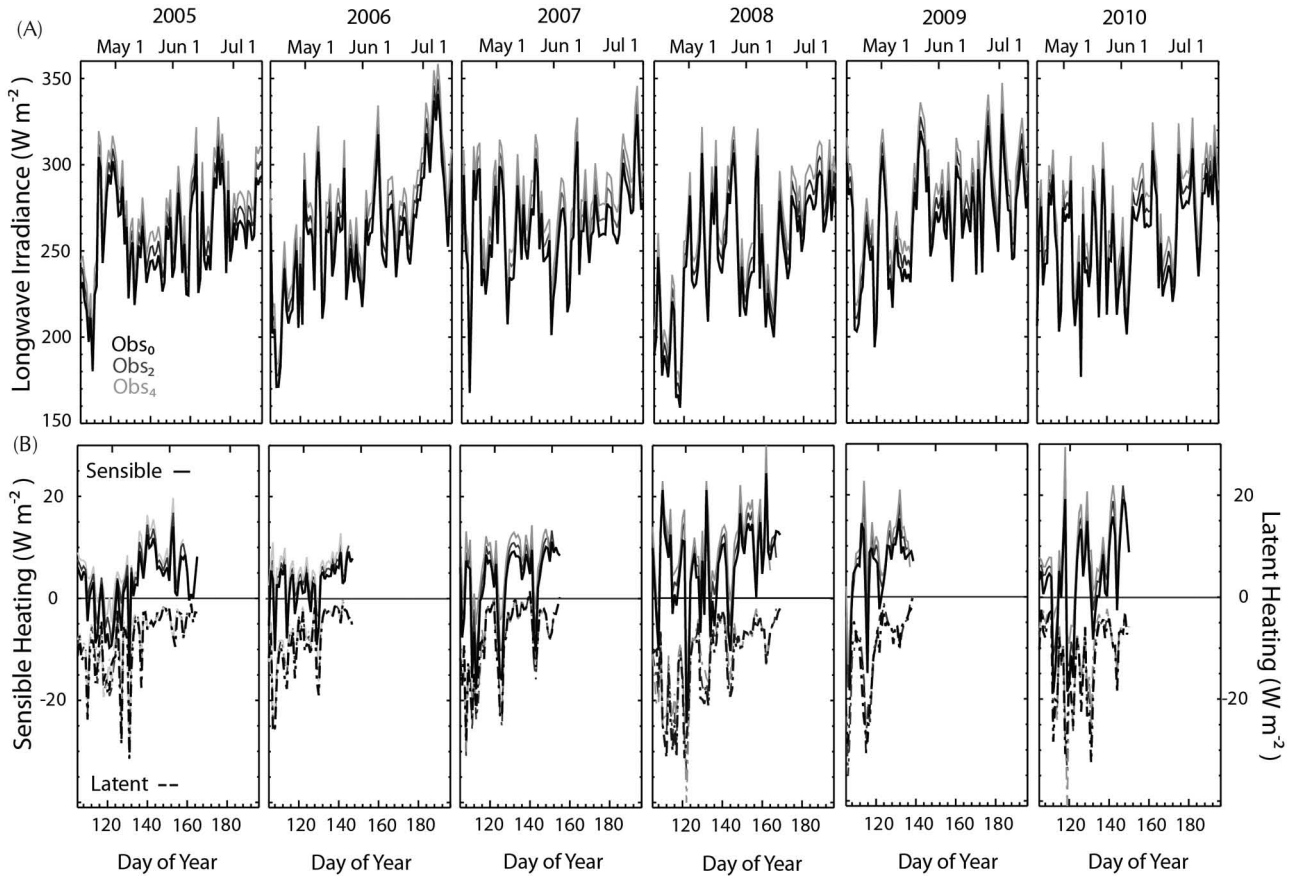


Figure 4. Time series of daily mean (a) longwave irradiance and (b) sensible heating and latent heating, for 2005 through 2010. Observed longwave irradiance is recorded at the subalpine tower; increases in downwelling longwave with temperature increases of 2°C and 4°C are shown by the lighter gray lines. Sensible and latent heating are simulated by SNOBAL. Lines end on modeled SAG date.

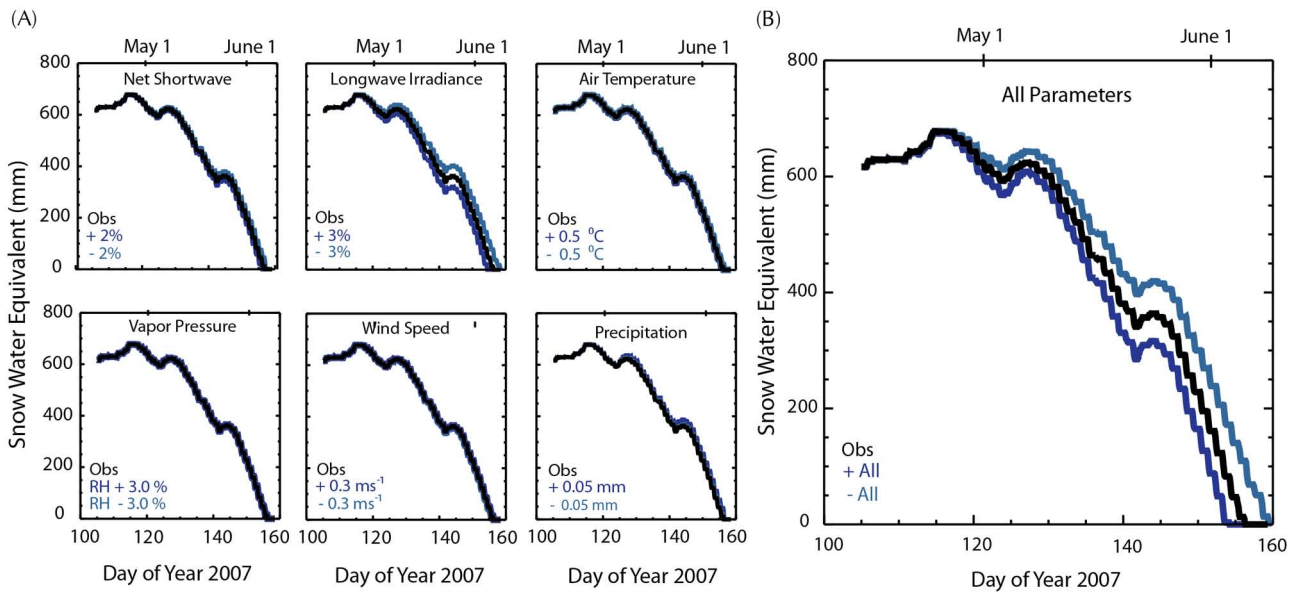


Figure 5. Modeled daily mean SWE evolution for ranges in (a) instrument accuracy and (b) maximum total uncertainty due to instrumentation measurement.

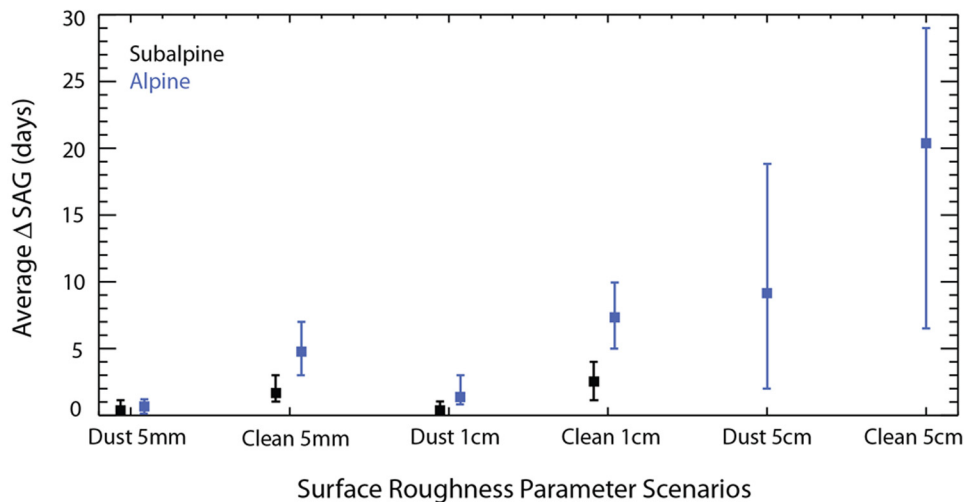


Figure 6. Average change in snow-all-gone date (Δ SAG) relative to the standard 1 mm roughness value for variations to the SNOBAL surface roughness parameter, error bars show maximum and minimum number of advanced days melt.

clean case at both sites, for a modeled clean snowpack increases in surface roughness can enhance melt by 3 to 7 days at the alpine site and 1 to 4 days at the subalpine site. The cumulative impacts from increased turbulent transfer at the surface in the presence of dust are reduced due to shorter snow duration.

[26] At the alpine site a marked increase in Δ SAG occurs between 1 and 5 cm increased surface roughness where large difference in melt-out date occurs. The larger Δ SAG for 1 and 5 cm roughness occur for both the dust and clean cases, driven by greater wind speeds in the alpine. The use of 1 mm constant surface roughness in the model is reasonable as these results indicate the model is not highly sensitive to changes in surface roughness until roughness values increase beyond those commonly observed for alpine snow cover in general, and for observed surface roughness at both of our study sites.

3.5. Snow Cover Duration

[27] We present the time series of snow water equivalent during the ablation seasons of 2005 through 2010 for the subalpine and alpine site (Figure 7). The ablation season is defined here as that between 15 April (near average peak SWE for the region) and date of SAG.

[28] The clean snowpack is modeled by removing the minimum and maximum RF due to dust, then averaging the daily values of these two scenarios to represent a conservatively clean snowpack (C_0); without direct observation of zero-dust conditions, this is our best understanding of the evolution of the snowpack in the absence of dust. The difference between when the D_0 and C_0 time series arrive at SAG (Δ SAG $_{D_0,C_0}$) indicates the number of days that dust RF advances complete melt under observed meteorological conditions.

[29] The greatest Δ SAG $_{D_0,C_0}$ of 51 days (subalpine) and 44 days (alpine) occurred in 2009 when the end of year dust concentration was 5–20 \times greater than concentrations in 2005 through 2008. The next largest divergence of 48 days (subalpine) and 37 days (alpine) occurred in 2010,

the next largest dust concentration year. The years with lower dust concentrations; 2005, 2007, and 2008 still show Δ SAG $_{D_0,C_0}$ of 28–34 days (subalpine) and 23–27 days (alpine).

[30] Dust radiative forcing exerts its strongest impact on Δ SAG in years with greater SWE accumulation, as dust-driven divergence in melt rates has more mass over which to influence duration of snow cover [Painter *et al.*, 2007]. This is illustrated by a comparison of 2005 (a high SWE, low dust year) and 2006 (low SWE, high dust). In 2005, Δ SAG $_{D_0,C_0}$ was 28 days (subalpine) and 23 days (alpine), whereas for 2006 the Δ SAG $_{D_0,C_0}$ was 31 days (subalpine) and 21 days (alpine). At the alpine site this was the smallest difference between the D_0 and C_0 cases, even though 2006 had a higher end-of-year dust concentration than did 2005. The higher peak SWE in 2005 relative to 2006 resulted in the small difference in Δ SAG $_{D_0,C_0}$ between the two years despite the increase in dust concentration and radiative forcing in 2006. A larger Δ SAG $_{D_0,C_0}$ would have been possible in 2006 with greater SWE accumulation.

[31] While there is interannual variability in the influence of dust RF on SAG, over the 6-year record, Δ SAG $_{D_0,C_0}$ can appear to increase linearly with the end-of-year dust concentration for each site (Figure 8; R^2 values of 0.94 and 0.95 at the subalpine and alpine site, respectively). However, given the nonlinear response of reduction of albedo to increases in dust concentration, we would expect that the relationship between Δ SAG $_{D_0,C_0}$ and dust concentration would likewise be nonlinear. Indeed, with the subalpine and alpine data taken together, the plot of Δ SAG $_{D_0,C_0}$ to dust concentration suggests a logarithmic form, which is more consistent with our understanding of optical responses. Future data from the SBBSA will allow us to more robustly populate this plot.

3.6. Influence of Temperature Increases

[32] The differences of C_2 and C_4 SAG from C_0 SAG (Figure 7) indicate the number of days that the temperature increases would advance loss of snow cover in the absence of dust (Δ SAG $_{C_2,C_0}$ and Δ SAG $_{C_4,C_0}$, respectively). The

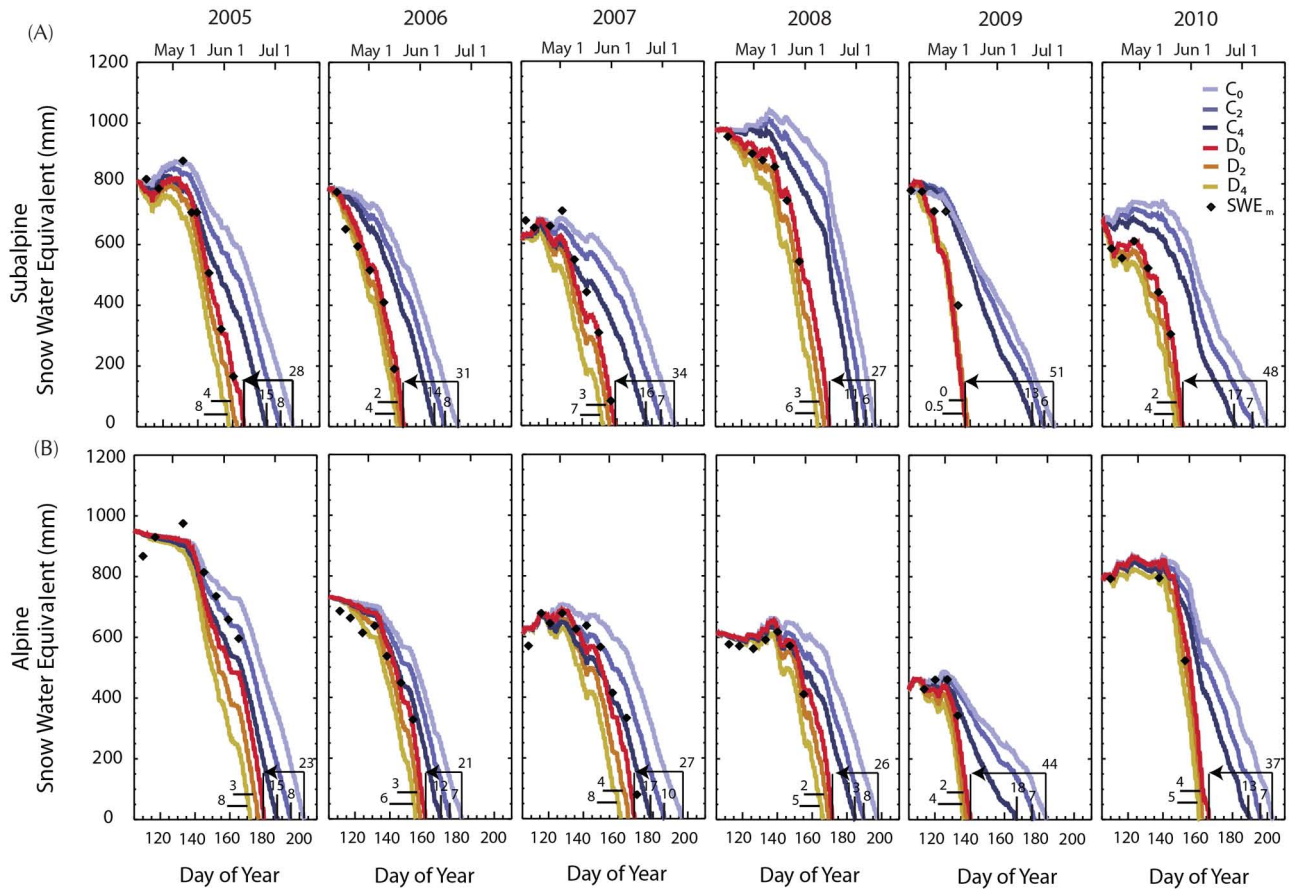


Figure 7. Daily mean SWE during the ablation season at the (a) subalpine and (b) alpine for all scenarios. Numbers by the C_2 , C_4 , and D_0 indicate number of days advanced melt from the C_0 case. Numbers by the D_2 and D_4 curves represent advanced melt from the D_0 case. Modeled SWE for D_0 closely matches point measurements of SWE (black triangles) for observed conditions (red curve) in almost all cases.

differences of D_2 and D_4 SAG from D_0 SAG represent the number of days temperature increases would further shorten snow cover in the presence of dust ($\Delta SAG_{D_2, D_0}$ and $\Delta SAG_{D_4, D_0}$, respectively).

[33] Temperature increases of 2°C and 4°C under dust-free scenarios induce $\Delta SAG_{C_2, C_0}$ and $\Delta SAG_{C_4, C_0}$ of 6 to 18 days—a lesser melt forcing than the observed dust radiative forcing in this region (21 to 51 days). Combined with

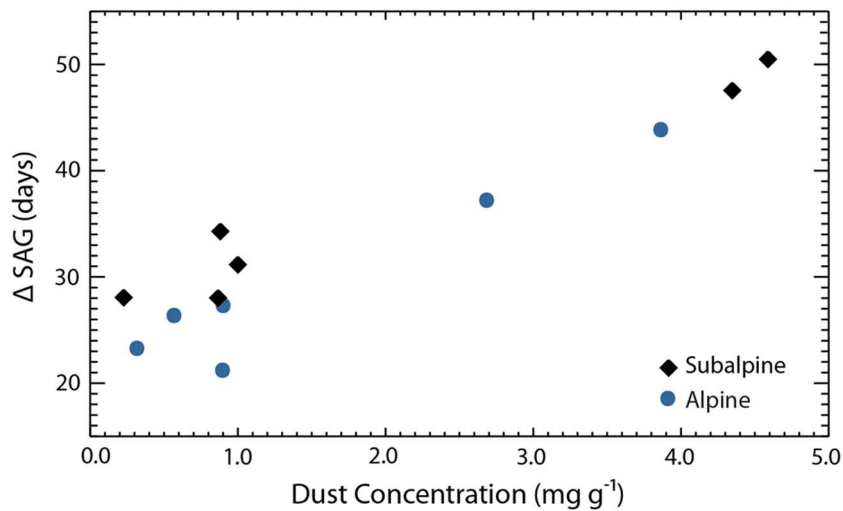


Figure 8. Change in snow-all-gone date (ΔSAG) with end of year dust concentrations. R^2 values are 0.94 and 0.92 at the subalpine and alpine site, respectively.

observed dust conditions, the increases in temperature shortened snowcover duration by 0 to 8 additional days ($\Delta\text{SAG}_{D_2,D_0}$, $\Delta\text{SAG}_{D_4,D_0}$). The reduced impact of increased temperature under dusty conditions is due to the reduced snow cover duration over which the increased sensible heating and longwave irradiance can affect a difference in SAG. The lowest melt forcing by increased temperature in the dusty case occurred in 2009 at the subalpine site, corresponding to the greatest mean dust radiative forcing. In these scenarios, $\Delta\text{SAG}_{D_2,D_0}$, $\Delta\text{SAG}_{D_4,D_0}$ were <1 day.

3.7. Snowpack Outflow

[34] In addition to SWE, daily mean “snowpack outflows” were also modeled (Figure 9). Because SNOBAL simulates only melt and sublimation at a point and does not account for infiltration into the soil column, transpiration by vegetation in or near the snow column, etc., we refer to the water leaving the bottom of the snowpack as outflow.

[35] Generally, the dust-driven outflows have a quasi-monotonic increase to a higher peak at the end of snow cover, and then melt-out occurs within days—on average 2.5 (subalpine) to 3.5 days (alpine) after peak outflow. The clean snow cases reach a lower peak 1 to 2 weeks after the dust cases with a less rapid decrease to melt-out, on average 19 (subalpine) to 13 days (alpine) after peak outflow occurs, as energy fluxes to the surface decrease. In 2006, a rain-on-snow event was predicted for the C_4 scenario at the

subalpine site (after melt-out in the dust cases). This was modeled as snow for other scenarios and produced a peak outflow higher than any of the dust peaks. Similar late season rain-on-snow events with smaller magnitude also occur in 2009 at the subalpine site and 2010 at both sites. These are functions of air temperature and precipitation phase change prediction by the model, which utilizes temperature during precipitation events to determine precipitation type.

[36] In all years at both sites, annual outflow flux in the dust cases exceeds that of the clean cases (Figure 10). In the heaviest dust concentration year (2009), the D_0 outflow (0.97 kg m^{-2}) was more than double the C_n outflow (0.44 kg m^{-2}) at the subalpine site. On average, D_0 outflow over all years is 0.71 and 0.49 kg m^{-2} (subalpine, alpine), whereas average C_n outflow is 0.39 and 0.27 kg m^{-2} (subalpine, alpine).

[37] The variation in timing of peak outflow between dust and clean scenarios has implications for water resources and water resource management. In addition to danger from flooding, higher melt rates and increases in the magnitude of peak runoff can impact soil moisture storage and reduce the time period over which critical water management decisions are made. A longer snow-free season likely increases the amount of water lost to evapotranspiration and reduces available water supply [Painter *et al.*, 2010]. This is especially pertinent in this region as the majority of flow in the Colorado River comes from the melting of high

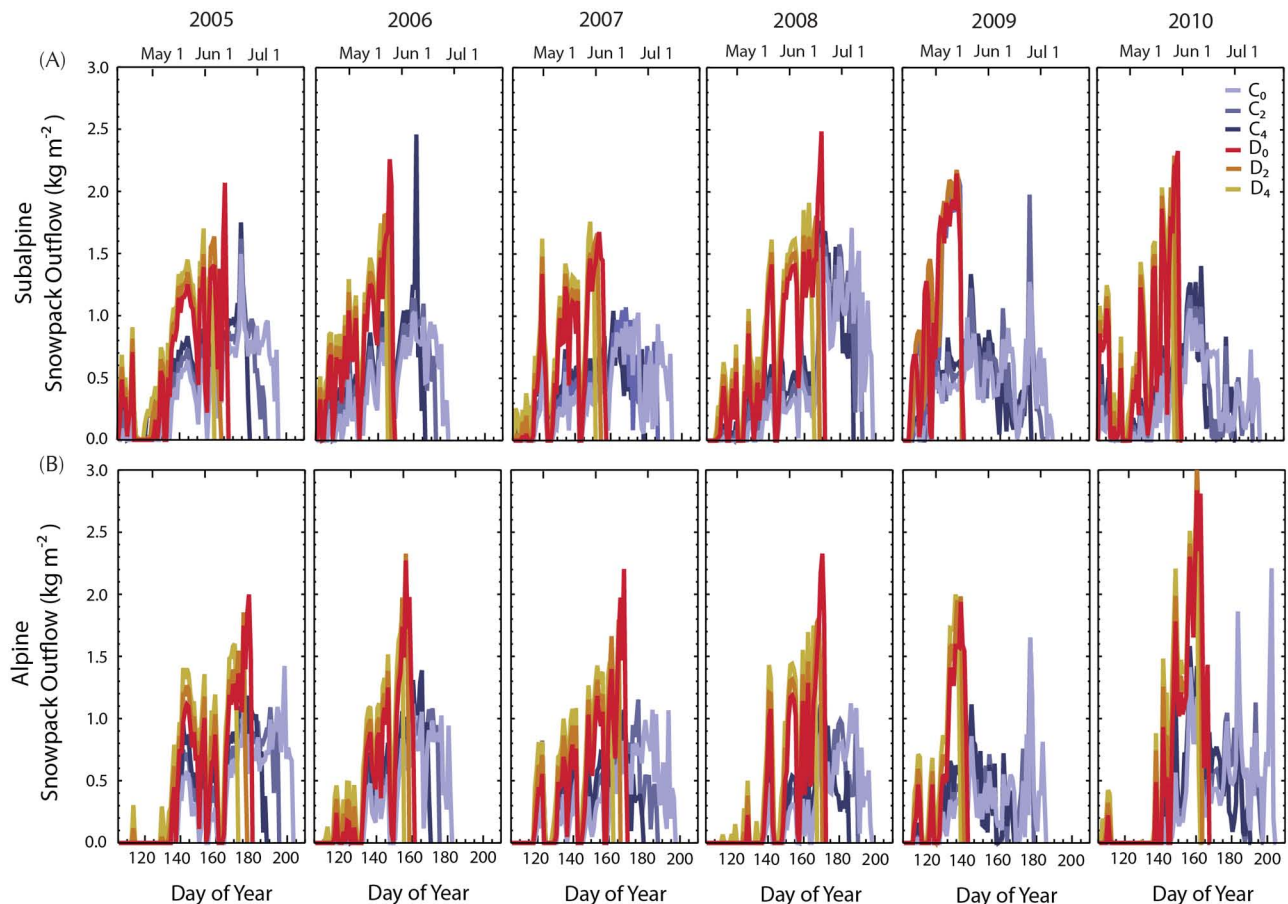


Figure 9. Time series of daily mean snowpack outflow over the ablation season at (a) subalpine and (b) alpine sites for all scenarios.

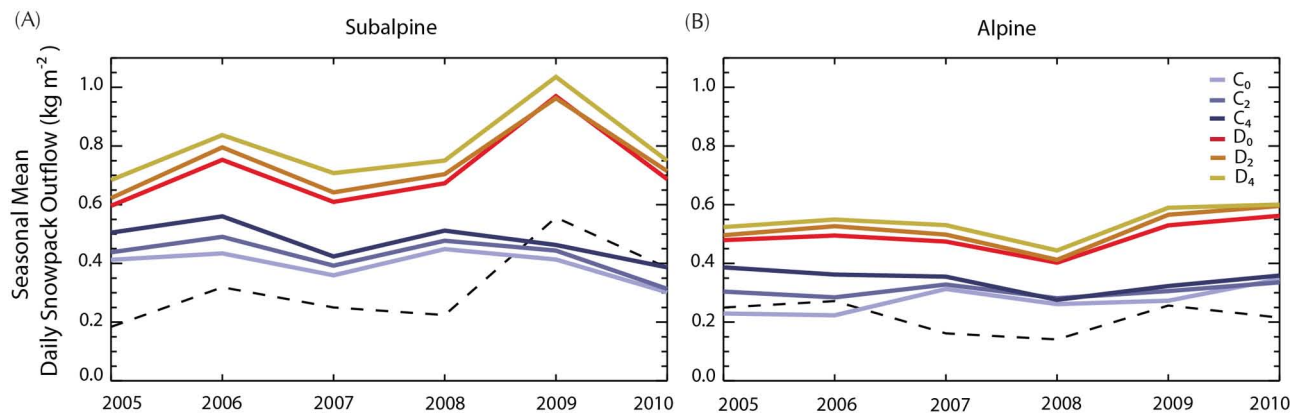


Figure 10. Mean daily snowpack outflow for all scenarios at the (a) subalpine and (b) alpine, with the difference between the D_0 and C_0 snowpack outflows represented by the dashed line.

elevation snow cover [Christensen *et al.*, 2004]. Water availability may also be impacted if the majority of the water melts over a shorter period of time and there is insufficient reservoir storage to hold the accelerated flow and reservoir spillage is unavoidable. Additionally, earlier removal of snow cover coupled with increasing temperature has the potential to impact alpine vegetation patterns, with a shift toward earlier, more spatially coincident greening and flowering [Steltzer *et al.*, 2009].

4. Concluding Remarks

[38] Modern levels of dust deposition on the mountain snowpack are a relatively new phenomenon in this region over the last 150 years [Neff *et al.*, 2008; Painter *et al.*, 2010]. Over the 6-year record at our study area we have observed an increase in the number of dust events with substantial interannual variability in dust loading. Painter *et al.* [2007] found that dust in snow advanced melt-out date by up to 35 days in the springs of 2005 and 2006. We find that in high dust concentration years melt-out date can be advanced by up to 51 days.

[39] Enhanced snowmelt rates increase the rate of snowpack outflow, which can impact water supply operations. Faster melt also lengthens the snow-free season, when evapotranspiration rates are highest. Painter *et al.* [2010] found that dust RF impacts annual runoff volume of the Colorado River at Lee's Ferry, AZ, by 5% (~ 1.0 billion m^3) on average. Their study was conducted using a snow albedo parameterization that comes from 2005–2008, and does not include the exceptionally low albedos observed in 2009 and 2010—thus the runoff impacts of dust deposition may be even greater than estimated.

[40] While our results indicate that temperature does not have as large an impact on melt in the presence of dust we recognize that this is a relatively simple treatment of temperature increase and emphasize that this study investigates the relative forcings of snowmelt by dust radiative forcing and temperature increases for the same snowpack and only in the snowmelt season. These results do not address how climate change may impact alpine snow cover in other areas that do not experience as high of dust concentrations, neither does it address other impacts such as changing precipitation patterns and more precipitation falling as rain rather than snow that would result from a warming climate.

[41] Over our relatively short record we have observed that dust deposition can be highly variable; as discussed above, at our sites the number of dust deposition events increased during the period 2005 through 2010, yet dust concentrations have varied by more than an order of magnitude during those years but not in concert with the steady increase in number of events. This is due in part because climate, land cover, and atmospheric circulation, which vary at multiple spatial and temporal scales, impact dust emission and loading. In addition to natural variability, human impacts such as changes in land use are contributing to changes in dust emission. This variability may increase with ongoing regional warming. Warming in the southwestern US is likely to increase dust emission and loading to the mountains of the CRB through drought, disturbance, and desertification [Munson *et al.*, 2011]. It is important to understand the interannual variability of dust deposition to the mountain snow cover to better understand the potential long-term impacts. The results presented here have important implications not just for runoff timing and magnitude and water supply management, but also for power generation, alpine phenology, forest fire regimes, and recreation interests.

[42] **Acknowledgments.** This work was funded by the National Science Foundation grants ATM0432327 and ATM0431955, and NASA project NNX10AO97G. We acknowledge the assistance of Andrew Barrett in data processing. Part of this work was performed at the Jet Propulsion Laboratory, California Institute of Technology under a contract with NASA. We thank Jeff Dozier, Steve Warren, and an anonymous reviewer for their suggestions that improved this manuscript.

References

- Ball, F. K. (1954), Dirt polygons on snow, *Weather*, 9, 322–323.
- Barnett, T. P., and D. W. Pierce (2009), Sustainable water deliveries from the Colorado River in a changing climate, *Proc. Natl. Acad. Sci. U.S.A.*, 106, 7334–7338, doi:10.1073/pnas.0812762106.
- Brock, B. W., I. C. Willis, and M. J. Sharp (2006), Measurement and parameterization of aerodynamic roughness length variations at Haut Glacier d'Arolla, Switzerland, *J. Glaciol.*, 52, 675–688, doi:10.3189/172756500781832675.
- Christensen, N. S., A. W. Wood, D. P. Lettenmaier, and R. N. Palmer (2004), Effects of climate change on the hydrology and water resources of the Colorado River Basin, *J. Hydroclimatol.*, 6, 337–363.
- Fassnacht, S. R., M. W. Williams, and M. V. Carrao (2009), Changes in the surface roughness of snow from millimetre to metre scales, *Eco. Complex.*, 6, 221–229, doi:10.1016/j.ecocom.2009.05.003.

- Hansen, J., and L. Nazarenko (2004), Soot climate forcing via snow and ice albedos, *Proc. Natl. Academy Sci. U.S.A.*, *101*, 423–428.
- Jackson, B. S., and J. J. Carroll (1978), Aerodynamic roughness as a function of wind direction over asymmetric surface elements, *Bound.-Layer Meteorol.*, *14*, 323–330, doi:10.1007/BF00121042.
- Konzelmann, T., R. S. W. van de Wal, W. Greuell, R. Bintanja, E. A. C. Henneken, and A. Abe-Ouchi (1994), Parameterization of global and longwave incoming radiation for the Greenland Ice Sheet, *Global Planet Change*, *9*, 143–164, doi:10.1016/0921-8181(94)90013-2.
- Marks, D., and J. Dozier (1992), Climate and energy exchange at the snow surface in the alpine region of the Sierra Nevada 2. Snow cover energy balance, *Water Resour. Res.*, *28*, 3043–3054.
- Marks, D., J. Dozier, and R. E. Davis (1992), Climate and energy exchange at the snow surface in the alpine region of the Sierra Nevada 1. Meteorological measurements and monitoring, *Water Resour. Res.*, *28*, 3029–3042.
- Marks, D., J. Kimball, D. Tingey, and T. Link (1998), The sensitivity of snowmelt processes to climate conditions and forest cover during rain-on-snow: A case study of the 1996 Pacific Northwest flood, *Hydrological Processes*, *12*, 24.
- Munson, S. M., J. Belnap, and G. S. Okin (2011), Responses of wind erosion to climate-induced vegetation changes on the Colorado Plateau, *Proc. Natl. Acad. Sci. U.S.A.*, *108*, 3854–3859, doi:10.1073/pnas.1014947108.
- Neff, J. C., A. P. Ballantyne, G. L. Farmer, N. M. Mahowald, J. L. Conroy, C. C. Landry, J. T. Overpeck, T. H. Painter, C. R. Lawrence, and R. L. Reynolds (2008), Increasing eolian dust deposition in the western United States linked to human activity, *Nat. Geosci.*, *1*, 189–195, doi:10.1038/ngeo133.
- Painter, T. H. (2011), Comment on: S. K. Singh, Anil V. Kulkarni, and Bajrang S. Chaudhary, Hyperspectral analysis of snow reflectance to understand the effects of contamination and grain size, *Annals of Glaciology* *51*(54) 2010, *J. Glaciol.*, *57*, 183–185, doi:10.3189/002214311795306646.
- Painter, T. H., A. P. Barrett, C. C. Landry, J. C. Neff, M. P. Cassidy, C. R. Lawrence, K. E. McBride, and G. L. Farmer (2007), Impact of disturbed desert soils on duration of mountain snow cover, *Geophys. Res. Lett.*, *34*, L12502, doi:10.1029/2007GL030284.
- Painter, T. H., J. S. Deems, J. Belnap, A. F. Hamlet, C. C. Landry, and B. Udall (2010), Response of Colorado River runoff to dust radiative forcing in snow, *Proc. Natl. Acad. Sci. U.S.A.*, *107*, 17125–17130, doi:10.1073/pnas.0913139107.
- Painter, T. H., S. M. Skiles, J. S. Deems, A. C. Bryant, and C. C. Landry (2012), Dust radiative forcing in snow of the Upper Colorado River Basin: 1. A 6 year record of energy balance, radiation, and dust concentrations, *Water Resour. Res.*, *48*, W07521, doi:10.1029/2012WR011985.
- Pluss, C., and R. Mazzoni (1994), The role of turbulent heat fluxes in the energy balance of high Alpine snow cover, *Nord. Hydrol.*, *25*, 25–38, doi:10.2166/nh.1994.002.
- Poggi, A. (1976), Heat balance in the ablation area of the Ampere Glacier (Kerguelen Islands), *J. Appl. Meteorol.*, *16*, 48–55, doi:10.1175/1520-0450.
- Rhodes, J. J., R. L. Armstrong, and S. G. Warren (1987), Mode of formation of “ablation hollows” controlled by dirt content of snow, *J. Glaciol.*, *33*, 135–139.
- Sedlar, J., and R. Hock (2009), Testing longwave radiation parameterizations under clear and overcast skies at Storglaciären, Sweden, *The Cryosphere*, *3*, 75–84, doi:10.5194/tc-3-75-2009.
- Singh, S. K., A. V. Kulkarni, and B. S. Chaudhary (2010), Hyperspectral analysis of snow reflectance to understand the effects of contamination and grain size, *Ann. Glaciol.*, *51*, 83–88, doi:10.3189/172756410791386535.
- Steltzer, H., C. C. Landry, T. H. Painter, J. Anderson, and E. Ayres (2009), Dust-induced early snowmelt synchronizes phenology across an alpine landscape, *Proc. Natl. Acad. Sci. U.S.A.*, *106*, 11629–11634, doi:10.1073/pnas.0900758106.